TECHNICAL MEMORANDUM

X-509

CONVECTIVE HEAT TRANSFER TO A LIFTING FLAT-FACED-CONE ENTRY BODY

By James E. Terry

Ames Research Center
Moffett Field, Calif.

[redacted]

NATIONAL AERONAUTICS AND SPACE ADMINISTRATION
WASHINGTON
May 1961

[redacted]

NATIONAL AERONAUTICS AND SPACE ADMINISTRATION

TECHNICAL MEMORANDUM X-509

CONVECTIVE HEAT TRANSFER TO A LIFTING FLAT-FACED-CONE ENTRY BODY*

By James E. Terry

SUMMARY

Heat-transfer and pressure distributions were measured on a flat-faced-cone representative of a family of blunt lifting bodies previously studied by Davy and Seiff. The configuration was designed to have a maximum lift-drag ratio of approximately 1/2. Measurements were made at nominal Mach numbers of 4 and 5. (Pressures were measured at M = 3 also.) Free-stream Reynolds numbers varied from 0.50 million to 0.88 million based on base height. Angles of attack varied from -20° to +15°, and angles of sideslip varied from 0° to 15°.

Measured heat-transfer distributions showed that at the design attitude, heat transfer was maximum in the region of the upper corner approximately 30 percent greater than at the center of the flat face. The latter point has the low heat-transfer rate associated with a flat face, namely about equal to the stagnation point heating on a sphere with radius equal to one and one-half times the model base radius. On the afterbody, the heat transfer fell to as low as 1/20 of the maximum heating rate on the upper surface and 3/10 on the lower surface. The data are in reasonably good agreement with a Falkner-Skan flow solution based on a measured pressure distribution. Excellent agreement was obtained between theory and experiment for total heat input (exclusive of base heating). Minimum total heat input occurred at an angle of attack of zero with the corresponding lift-drag ratio of about 0.45.

Exploratory flow visualization studies were made at a Mach number of 3 in an attempt to find the cause of certain anomalies in the measured heat-transfer distributions. Several separated flow regions were shown to exist on the upper surface at high angles of attack. At large negative angles of attack, a region of low skin friction was shown on the lower surface which confirmed the very low heat transfer coefficients measured for that area.

*Title, Unclassified

[redacted]

[redacted]

INTRODUCTION

It is well known that aerodynamic heating to a body entering the earth's atmosphere at high velocities can be materially reduced by body blunting. Recent studies by Chapman (ref. 1) have also shown that decelerations and peak heating rates can be reduced by the use of lift during the entry. In addition, the guidance problem is simplified by use of lift since the entry corridor depth can be increased to several times it's zero lift depth (ref. 2). Some selection of the landing site can be obtained from the ability of a lifting vehicle to manuever.

The aerodynamic characteristics of a family of blunt lifting bodies have been studied by Davy and Seiff (ref. 3). Of this family, one particular configuration designed for an L/D of approximately 1/2 was studied experimentally. A photograph of a model of this configuration is shown in figure 1. This paper deals with the convective heat transfer to that configuration at Mach numbers of 4 and 4.9 and free-stream Reynolds numbers (referenced to base height) of 0.50 to 0.88 million. Angles of attack were varied from -20° to $+15^\circ$ and angles of sideslip were varied to 15°. Pressure distributions were obtained for the same test conditions and at a Mach number of 3 also. Comparisons were made between experimental heat-transfer data and both a Falkner-Skan flow solution based on measured pressure distributions and a zero pressure gradient solution.

SYMBOLS

b	base height, ft
c	specific heat of model material, $\frac{\text{Btu}}{\text{lb } ^\circ\text{R}}$
C_p	pressure coefficient
c_p	specific heat of air at constant pressure, $\frac{\text{Btu}}{\text{lb } ^\circ\text{R}}$
d	density of model material, $\frac{\text{lb}}{\text{ft}^3}$
D	drag, lb
E	Euler number, $\frac{x}{u_e}\frac{du_e}{dx}$
h	heat-transfer coefficient, $\frac{\text{Btu}}{\text{ft}^2 \text{ sec } ^\circ\text{R}}$
k	thermal conductivity of model material, $\frac{\text{Btu}}{\text{sec ft } ^\circ\text{R}}$
L	lift, lb

[redacted]

l length of flow path from stagnation point, ft

M Mach number

N_{ST} Stanton number, $\frac{h}{c_p \rho u}$

Nu Nusselt number, $\frac{hl}{k_w}$

Pr Prandtl number, $\frac{c_p \mu}{k}$

q heating rate, $\frac{Btu}{ft^2 \text{ sec}}$

Re_b Reynolds number, $\frac{\rho u b}{\mu}$

Re_l Reynolds number, $\frac{\rho_w u_e l}{\mu_w}$

r length of radius vector in spherical coordinates, ft

T temperature, ^oR

t time, sec

u velocity, ft/sec

x distance measured along surface from intersection of cone axis and front face, ft

α angle of attack

β angle of sideslip

θ angle between reference axis and radius vector in spherical coordinates

μ viscosity, $\frac{lb}{ft \text{ sec}}$

ρ air density, $\frac{slugs}{ft^3}$

τ model wall thickness, ft

φ meridian angle in spherical coordinates

[redacted]

Subscripts

e	evaluate at edge of boundary layer
eq	equilibrium value
s	stagnation value
w	evaluate at wall temperature
2	evaluate behind normal shock
∞	free-stream values

THEORY

Heat-transfer coefficients for the configuration shown in figure 2 were estimated from Falkner-Skan flow (also called wedge flow or Hartree flow) and flat-plate theories for supersonic compressible flow modified by Mangler transformations to account for three-dimensional effects. Falkner-Skan flow has a local stream velocity at the edge of the boundary layer given by:

$$u_e \propto l^E \tag{1}$$

Theories utilizing solutions to the boundary-layer equations for this type of flow are presented in references 4 and 5. These theories differ only in corrections for Mach number, and in the fact that reference 5 allows for the use of Sutherland's viscosity variation while reference 4 makes use of a simple power law. For the test conditions, these differences were small. The Falkner-Skan solution presented in this report was calculated by the technique presented in reference 5. The flat-plate solution was calculated by the same technique as the Falkner-Skan flow solution except that the pressure gradient was taken as zero.

To convert the two-dimensional solutions to three-dimensional axisymmetric solutions the Mangler transformation (ref. 5) was used. Since the configuration tested was not axisymmetric, it was assumed that each meridian could be treated as a line on an axisymmetric body. The local body radius was taken to be the distance (normal to the free-stream velocity vector) from the cone axis to the body surface. With the assumption that streamlines were along meridian lines, the local velocity gradients were determined from measured pressure distributions. It should be pointed out that the gradients in the corner regions were large and not well defined.

[redacted]

The stagnation-point heat-transfer parameter has been shown (ref. 6) to be:

$$\frac{Nu}{\sqrt{Re_l}} = 0.67 \left(\frac{\rho_s \mu_s}{\rho_w \mu_w}\right)^{0.4} \tag{2}$$

for stagnation temperatures below that necessary for dissociation. For a constant specific heat, the heat-transfer coefficient is then:

$$h_s = \frac{0.67}{Pr_w} \left(\frac{\rho_s \mu_s}{\rho_w \mu_w}\right)^{0.4} \left(\rho_w \mu_w \frac{du}{dx}\right)^{0.5} c_p \tag{3}$$

Thus the heat-transfer coefficient is a function of the square root of the velocity gradient. The velocity gradient could not be obtained from Newtonian theory since the front face was flat. The configuration was not axisymmetric, so the velocity gradient varied with meridian angle. Stagnation-point velocity gradient was calculated from pressures measured in the $\varphi = 90^\circ$ plane (see fig. (2)).

EXPERIMENT

Models

Two models were used in the experiment: one was instrumented to measure pressure, while the other was instrumented to measure temperature. Instrumentation locations (identical on the two models) are shown in figure 2. The pressure-distribution model was made of aluminum. Holes were drilled normal to the model surface to intersect a central cavity. Stainless-steel tubing of 0.022 inside diameter was passed through the cavity and bonded into the holes. The tubes were potted in the cavity with an epoxy potting compound and trimmed flush with the surface to form the pressure orifices. Plastic tubing was used to connect the tubes to a manometer board.

The heat-transfer model was an electroformed nickel shell with the wall thickness varying from about 0.015 inch on the flat face to about 0.012 inch on the conical afterbody. The circumferential variation of wall thickness did not exceed 0.001 inch. Copper-constantan thermocouples were soft soldered into the shell as shown in figure 2. A laminated-fabric-base plastic base plug insulated the model from the sting. Both models were finished with 2/0 emery paper; however, some local scratches from rougher papers remained. Nevertheless, the finish was sufficiently smooth that no evidence of turbulent flow could be found in the shadowgraphs for any test condition. A photograph of the heat-transfer model after testing is shown in figure 1.

Instrumentation and Test Procedure

The pressure and heat-transfer measurements were made in the Ames 10-Inch Heat Transfer Wind Tunnel. This tunnel is a continuous flow, variable pressure, variable temperature type with a Mach number range of 3 to 5. Maximum total pressure is about 85 psia and the tunnel is usually operated at a total temperature between 650° R and 750° R. Flow visualization studies were conducted in an 8- by 7-inch wind tunnel. This tunnel is an unheated blowdown type with fixed nozzle blocks for a Mach number of 3. Total pressure can be varied from about 35 to 100 psia.

The pressure data were recorded on manometers with manometer fluids appropriate to the local pressures. High pressures were recorded on mercury manometers which were referenced to atmospheric pressure. A mercury barometer was used to measure atmospheric pressure. Low pressures were recorded on dibutylphthalate manometers which were referenced to a vacuum. The vacuum reference was measured with a McLeod gage. In all cases the reference pressure was less than 100 microns of mercury. At least 15 minutes were allowed after each change in a test parameter for the manometer to stabilize. Pressures were recorded by photographing the manometer.

The heat-transfer model was cooled by injecting liquid nitrogen into the tunnel settling chamber upstream of the nozzle. Model wall temperatures were depressed about 80° R but an isothermal surface could not be obtained with this cooling method. Oscillograph recordings were made of the temperatures and time derivatives of the temperatures when the nitrogen flow was stopped. Only 12 channels of information could be recorded during a given run, so two runs were necessary for each test condition. The thermocouple output was amplified and recorded on one oscillograph. A differential analyzer took the time derivative of the amplifier output and this was simultaneously recorded on a second oscillograph. To prevent excessive length (and corresponding high resistance) of the thermocouple wire, it was necessary to locate the thermocouple cold junctions in a region of relatively high temperature. A reference thermocouple made from the same spool of wire as those in the model was used to measure the potential of the model thermocouple cold junctions with respect to ice water. Model wall temperatures were obtained from N.B.S. (ref. 7) calibrations of copper-constantan thermocouples and the sum of the outputs of the model and reference thermocouples. Model wall equilibrium temperatures were recorded after waiting at least 15 minutes after any change in the test conditions for the wall temperature to stabilize.

The pressure-distribution model was used in the flow visualization studies. A flourescent oil film technique as outlined in reference 8 was used. The oil and flourescent powder mix was painted on the model with a small brush and illuminated by two ultraviolet lamps. Kodacolor pictures were taken of the flow pattern about 3 to 5 minutes after the tunnel was started.

Test Conditions

Pressure-distribution tests were run at Mach numbers of 3.0, 4.0, and 4.9. Heat-transfer tests were run at 4.1 and 4.9. Free-stream Reynolds number was varied from 0.50 to 0.88 million referenced to model base height. For both pressure-distribution and heat-transfer tests at a Mach number of 4 and a Reynolds number of 0.8 million, the model was pitched in 5° increments from -20° to +15° and yawed in 5° increments to 15°. At other Mach numbers and Reynolds numbers, tests were run only at 0° angles of attack and sideslip. Flow visualization studies were run at a Mach number of 3.0 and a free-stream Reynolds number of 1.3 million at angles of attack of -20°, 0°, and +20° at 0° angle of sideslip.

Data Reduction and Accuracy

The heat balance equation for the model may be written:

$$q_{model} = q_{convection} + q_{conduction} + q_{radiation}$$

Radiation heat transfer was thought to be negligible. Conduction heat transfer was not negligible and will be discussed later; however, because the conduction could not be calculated accurately, it was neglected in the data reduction. For a thin-skinned model, the convective heat-transfer coefficient can then be written:

$$h = \frac{q}{T_{we} - T_w} = \frac{c d\tau}{T_{we} - T_w}\left(\frac{dT_w}{dt}\right)$$

The specific heat of the model material at the appropriate temperature was calculated from a polynomial fitted to the data of reference 9. If the surface area is assumed to be constant, the product $d\tau$ does not vary with temperature. This product was therefore taken to have its room temperature value. The density of pure nickel was obtained from reference 10. Model wall thickness was measured with a dial indicator at each thermocouple location prior to the thermocouple installation.

From calibrations of the recording equipment it was found that the response time of the temperature recording system was about 0.03 second. The response time of the temperature derivative recording system was about 0.3 second. The data were therefore read at 0.3 second after the liquid nitrogen was shut off. Timing pips were simultaneously recorded on both oscillographs to aid in interpretation of the data.

The accuracy of the data was estimated from the calibrations of the differential analyzer and recording equipment and from sensitivity and repeatability of the readout equipment. The estimated accuracies of the data are tabulated below:

T_w	$\pm 5.0^\circ$ R
$T_{we} - T_w$	$\pm 3.2^\circ$ R
dT_w/dt	$\pm 0.4^\circ$ R per sec
h	±6 percent of the stagnation point value
$c_p/c_{p_{max}}$	±0.005

In addition to the above measurement errors, conduction errors, estimated to be up to 30 percent of the stagnation-point heat-transfer coefficient, existed because of the nonisothermal surface. These errors will be discussed in the appendix. The history of the boundary layer over a nonisothermal model would be different from that over an isothermal model. Errors due to this fact were thought to be small for these tests and were not considered.

RESULTS AND DISCUSSION

Pressure Data

The pressure data obtained at a test Mach number of 4.0 are presented as the pressure-coefficient ratio versus body position in figure 3. Pressure distributions for the plane of symmetry at various angles of attack are presented in figure 3(a). Distributions for the $\varphi = 90^\circ$ plane at various angles of sideslip are presented in figure 3(b). The pressure distribution in the plane of symmetry at zero angle of attack was only slightly affected by sideslip. Similarly, the zero sideslip pressure distribution of the $\varphi = 90^\circ$ plane was only slightly affected by pitch.

Except at the corners, the variation of pressure coefficient ratio with Mach and Reynolds numbers through the range tested was smaller than the size of the symbols in figure 3. The variation with Mach number of pressure coefficient over the afterbody is shown to an enlarged scale in figure 4. It can be seen that for each meridian, the pressure coefficient at the shoulder was low at a Mach number of 3 and increased with increasing Mach number. Farther aft, the pressure coefficient on the top and side tended to be independent of Mach number. On the lower surface the pressure coefficient over the aft part tended to decrease with Mach number although the variation was small.

Heat-Transfer Data

The heat-transfer data are presented in terms of a dimensionless parameter $(N_{St}Re_b^{1/2}Pr^{2/3})_2$. All gas properties were evaluated at conditions behind a normal shock. Thus, for a given test condition, this parameter is equal to a constant times the heat-transfer coefficient. The data can be converted to h/h_s by dividing by the stagnation point heat-transfer parameter. With the assumption of a cold wall h/h_s is approximately equal to q/q_s.

The experimental heat-transfer distribution for the plane of symmetry and for the $\varphi = 90^\circ$ plane are shown in figures 5(a) and 5(b), respectively, and compared to Falkner-Skan and zero pressure gradient solutions. Inasmuch as the conical afterbody had nearly constant pressure along rays, the two solutions are the same for that region. As previously mentioned, velocity gradients in the corners were large and not well defined. These gradients were measured by taking the slope of the Mach number versus body position curves. The gradients obtained from successive fairings of the data were about the same for the upper and side corners. A fairly large difference in the gradients was obtained for the lower corner and the resulting variation in the theoretical heat-transfer coefficient is indicated by the shaded region in figure 5. The Falkner-Skan flow solution has been faired through a stagnation point value calculated from the theory of Fay and Riddell. As indicated by the dashed line, the flat-plate solution was simply faired from the points on either side of the stagnation point. It can be seen that both solutions indicate increased heating rates at the corners. When conduction effects (see appendix) are considered, it is felt that the Falkner-Skan flow solution is a reasonably good fit to the data.

It also can be noted that the last point on the lower surface shows an increase in heat transfer not predicted by theory. This rise was even more pronounced at negative angles of attack (see fig. 6(a)) and was also present in the $\varphi = 90^\circ$ plane. The last thermocouple in each meridian plane was about 0.4 inch from the base plug. Temperature distributions at the time of nitrogen shutoff indicate that the base plug was acting as a heat source. Conduction estimates were made for the last two thermocouples (thermocouples 13 and 14) in the $\varphi = 0^\circ$ plane for the temperature distributions for $\alpha = 0^\circ$ and -20° with the assumption that the base plug was acting as a heat source. The conduction estimates account for the observed increase in heat transfer near the base for $\alpha = 0^\circ$ but account for less than half the increase for $\alpha = -20^\circ$. Transition to turbulent flow could cause an increase in heat transfer but no evidence of turbulence could be found in any of the shadowgraphs. It was felt that the high heating rate at thermocouple 14 as compared to that at thermocouple 13 could be attributed to crossflow phenomena, and the flow visualization studies were conducted in an attempt to find the cause. At an angle of attack of -20°, a region of low skin friction was found to be

centered around thermocouple 13 and an increase in skin friction occurred approximately at thermocouple 14. This low skin friction region was not present at zero angle of attack where conduction estimates had accounted for the increased heating at thermocouple 14. A more complete discussion of the flow visualization studies will be made below.

The heat-transfer distribution in the plane of symmetry for angles of attack from -20° to $+15^\circ$ and zero sideslip is shown in figure 6(a). As shown in the pressure data, the zero angle of attack stagnation point was close to the intersection of the cone axis and the front face. This point will be called the nominal stagnation point. The heat transfer to the nominal stagnation point was approximately constant through the angle-of-attack range and therefore was useful as a standard with which to compare other heat-transfer rates. In the lower corner, peak heating varied from about 80 percent of nominal stagnation point heating at $\alpha = -20^\circ$ to about 135 percent at $\alpha = +15^\circ$. Peak heating in the upper corner varied from about 175 percent of nominal stagnation point heating at $\alpha = -20^\circ$ to about 115 percent at $\alpha = +15^\circ$. Under some conditions, heating rates on the afterbody were high. For example, heating rates on the afterbody in the $\varphi = 0$ plane exceeded 60 percent of nominal stagnation point heating at $\alpha = 15^\circ$. Heating rates approximately equal to the nominal stagnation point value were present on the line of tangency of the cone and corner at some angles. Negative heat-transfer coefficients were measured on the upper afterbody at the 10° and 15° angle-of-attack conditions. This observation can be explained as being due to conduction in the model shell, since the sides of the model shell were cooler than the top at the time the observations were made. Large transverse temperature differences were not required for conduction to exceed convection at these angles of attack because the pressures on the upper afterbody were low, resulting in low convective heat transfer.

Heat-transfer distributions for the $\varphi = 90^\circ$ plane at angles of sideslip to 15° are presented in figure 6(b). Two data points are presented at $x/b = 0$ for each sideslip angle other than zero. Only one side of the model was instrumented, so that each of these curves represents two runs. The spread between the two points is representative of the repeatability of the instrumentation and test technique.

Heat-transfer distributions for the plane of symmetry at various sideslip angles for zero angle of attack were determined but are not presented because the variation with sideslip of heat transfer in this plane was smaller than the accuracy of measurements. Therefore the distribution in figure 6(a) for zero angle of attack may be considered representative of the heating in the plane of symmetry at zero angle of attack for all sideslip angles of the test. Similarly, the distribution presented for the $\varphi = 90^\circ$ plane at zero sideslip is representative of heating in that plane for all angles of attack of the test.

The average heat-transfer parameter based on surface area not including base area is presented in figure 7 as a function of angle of attack. These values were obtained by means of a strip integration technique in which the body was divided in strips 45° wide with each strip centered on an instrumentation line. The heat-transfer coefficient was assumed to be constant across the strip and was faired between data points lengthwise of the strip. The data were extrapolated beyond the rearmost point to the base. With the assumption that the difference between recovery temperature and wall temperature is constant over the surface, total heat input may be found by multiplying the values in figure 7 by that temperature difference and the wetted area ($A = 2.61\ b^2$). This assumption is equivalent to the assumption that q/q_s equals h/h_s.

When it is assumed that no heat is transferred to the model from the support, the integrated total heat input is correct even if local coefficients are in error as a result of conduction. As previously mentioned, it is felt that some heat was being transferred from the base plug to the model. Because of a lack of instrumentation, the amount could not be evaluated accurately but estimates indicate that it was small compared to the total aerodynamic heating.

Minimum total heat input occurred at zero angle of attack which corresponds to an L/D of about 0.45. Total heat input increased approximately linearly for both positive and negative angles of attack although the slopes of the two lines were not equal. Total heat input would be about 106 percent of minimum for flight at $(L/D)_{max}$ ($L/D = 0.5$, $\alpha = 10°$). For flight at $L/D = 0$ ($\alpha = -17°$) total heat input would be about 121 percent of the minimum. The filled symbol represents an integration of the Falkner-Skan flow solution (upper curve) presented in figure 5. The agreement between theory and experiment is well within the integration accuracy and indicates that the total heat input may be predicted from theory.

It was thought desirable to know what fraction of the total heat input occurred to each of the three regions of the body, the flat face, the corner radius, and the afterbody. The flat face was found ($\alpha = 0$, $\beta = 0$) to contribute 13 percent of the total heat input. About 16 percent of the total was contributed by the corner radius. The remaining 71 percent of the total heating was on the afterbody. Thus it can be seen that a major portion of the total heat load occurs in regions of low heating rate. In addition, heating rate varies more with changes in flight attitude in these low rate regions than over the front face and corner (figs. 6(a) and 6(b)).

The variation of the heat-transfer parameter in the plane of symmetry with Mach number and Reynolds number is shown in figure 8. Although the variations are not purely random they are within the limits of estimated accuracy. The range of Mach and Reynolds numbers available for these tests was too small to allow general conclusions to be drawn as to their effects on heat transfer.

The variation of the heat-transfer parameter around the periphery at the beginning and end of the corner for different angles of attack at zero sideslip is shown in figure 9. At the beginning of the corner (fig. 9(a)) it can be seen that the highest heat-transfer rate sometimes occurred at the $\varphi = 45^\circ$ or $\varphi = 135^\circ$ position. Heat transfer to the $\varphi = 90^\circ$ and $\varphi = 135^\circ$ positions at the end of the corner (fig. 9(b)) were little affected by angle of attack. This is particularly noticeable at positive angles of attack where it might be thought that heating at $\varphi = 135^\circ$ should decrease as at $\varphi = 180^\circ$. A common assumption is that the peripheral variation in aerodynamic quantities around a body at an angle of attack can be approximated by a cosine curve. It can be seen that the peripheral variation on both sides of the corner is not well approximated by a cosine curve.

The peripheral variation of heat-transfer parameter at the beginning and end of the corner for different angles of sideslip at zero angle of attack is shown in figure 10. Sideslip had no effect on heating at the beginning of the corner on the leeward side of the model. The windward side had a large change between $\beta = 0^\circ$ and $\beta = 5^\circ$ followed by only a slight increase in heating for further increase in sideslip. Since only one side of the body was instrumented, each β actually represents data from two runs. As a result, each β has two data points at the $\varphi = 0^\circ$ and $\varphi = 180^\circ$ positions. The spread between the two points is indicative of the repeatability of the measurements. Heating at the end of the corner had a more uniform change with sideslip angle than did heating at the beginning of the corner. As in the previous figure, heating at the $\varphi = 45^\circ$ and $\varphi = 135^\circ$ points could not have been predicted by a cosine curve.

Flow Visualization Studies

The flow visualization pictures are shown in figure 11. Although the test conditions for the flow visualization studies ($M = 3$) were different than for the heat-transfer tests ($M = 4$), the flow patterns have been shown (see fig. 4 and previous discussion) to be similar. Over the rear part of the model, a group of well-defined evenly spaced lines can be seen. Very fine lines can also be seen over most of the model. Of the two sets, the fine lines appear to be the closer to the surface and are thought to approximate the direction of the surface pressure gradients. It is thought that the larger lines represent vortices which follow closely the streamlines at the edge of the boundary layer. Vortices have previously been observed in the boundary layers over swept wings (refs. 11 and 12). A certain critical crossflow Reynolds number is required for the formation of the vortices (ref. 12). Since the crossflow Reynolds number must approach zero near the plane of symmetry (at zero sideslip) and must vary over the rest of the model, a uniform vortex formation front would not be expected.

For these tests the pressure orifices were vented to the inside of the sting which was at some pressure higher than free stream. The resulting air jet from the orifice acted as a three-dimensional disturbance. As explained in reference 13, a three-dimensional disturbance will cause the formation of a pair of contra-rotating vortices with a stagnation region between. This pattern can be observed originating from each orifice on the afterbody.

Pictures of the side and bottom of the model at an angle of attack of -20° are shown in figures 11(b) and (c). A region of low skin friction, as indicated by a residual oil film remaining after several minutes running, can be seen immediately behind the corner in the bottom view. This region of low skin friction terminates approximately at the last orifice (corresponding to thermocouple 14). In figure 6(a), it can be seen that for this angle of attack, a very low heat-transfer coefficient was measured at thermocouple 13 (corresponding to the orifice in the low skin friction region) and a much higher value was measured at thermocouple 14. Except near the line of instrumentation, the edge of the low skin friction region appears to correspond approximately to the formation front of the vortices previously mentioned. While it is thought likely that the presence of the vortices in the boundary layer would increase the convective heat transfer, no conclusions could be drawn from these tests.

Pictures of both sides and the top of the model at an angle of attack of 20° are shown in figures 11(d), (e), and (f). Three distinct regions of separated flow can be seen in the top view. One region, roughly triangular in shape, is located just behind the corner and two more, symmetrically placed, are on the sides near the base of the model. The last two orifices (and corresponding thermocouples) on the upper surface were in the separated region behind the corner. In the heat-transfer tests, negative heat-transfer coefficients were measured at these locations at 10° and 15° angles of attack. As explained previously, the negative coefficients were felt to be the result of conduction heat transfer away from the point being larger than the aerodynamic heat transfer to the point. Very low aerodynamic heating would be expected in separated regions such as these. No information can be given concerning the separated regions near the base since there was no instrumentation in that area.

SUMMARY OF RESULTS

Pressure and heat-transfer distributions have been measured on a lifting flat-faced cone model at nominal Mach numbers of 4 and 5 and free-stream Reynolds numbers (based on model base height) from 0.50 million to 0.88 million, and at angles of attack from -20° to $+15^\circ$ and angles of sideslip to 15°. Additional pressure measurements were made at $M = 3$.

Measured heat-transfer distributions showed that the center of the front face had the relatively low heating rates associated with flat faces (approximately equal to the heating rate of a hemisphere of radius one and one-half times the model base radius). Somewhat higher heating rates were measured in the corner. Maximum heating rates in the corner varied from 30 percent higher than the center of the face at design attitude to 80 percent higher near zero lift.

The heat-transfer distribution was reasonably well predicted by a Falkner-Skan flow theory utilizing measured pressure distributions. Conduction errors present in the data could not be evaluated accurately but estimates indicated that correction of these errors would tend to improve the agreement between experiment and theory. Total heat input (neglecting base heating) was well predicted by the Falkner-Skan flow theory. Measured total heat input was minimum at zero angle of attack (the design attitude for $L/D \approx 1/2$) and increased approximately linearly for both positive and negative angles of attack.

Exploratory flow visualization studies were made at a Mach number of 3. Several separated flow regions were shown to exist on the upper surface at high angles of attack. At large negative angles of attack, a region of low skin friction was shown on the lower surface which confirmed the very low heat-transfer coefficients measured for that area.

Ames Research Center
National Aeronautics and Space Administration
Moffett Field, Calif., Feb. 28, 1961

APPENDIX

CONDUCTION

An isothermal surface could not be obtained with the cooling technique used. At the time data were taken the temperature varied over the model surface through a range of about 15° R. Conduction effects were also present in the equilibrium temperature measurements since the model was nonisothermal at that time. Therefore, two sources of error were present in the data reduction procedure outlined on page 7; q could be incorrect due to conduction at the time data were read and the equilibrium wall temperature was not equal to the recovery wall temperature. These errors could be either compensatory or additive. The conduction estimation technique used considered both sources of error.

For conduction calculations the front face may be considered as a flat plate for which the conduction equation is:

$$q = k_T \left(\frac{\partial^2 T}{\partial x^2} + \frac{\partial^2 T}{\partial y^2} \right) \tag{A1}$$

The conical afterbody may be considered as a surface in spherical coordinates as sketched below:

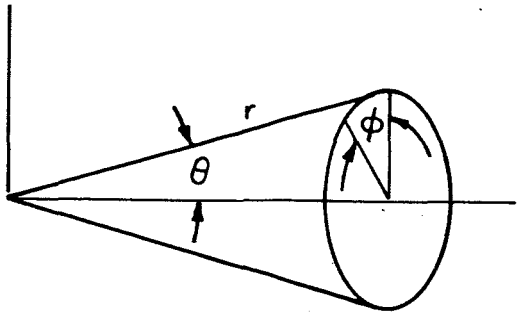

For a shell in which the wall thickness is constant but small compared to the radius of the cone, the equation for conduction in the shell is:

$$q = k_T \left(\frac{\partial^2 T}{\partial r^2} + \frac{1}{r} \frac{\partial T}{\partial r} + \frac{1}{r^2 \sin^2 \theta} \frac{\partial^2 T}{\partial \varphi^2} \right) \tag{A2}$$

It can be seen that a knowledge of both the first and second derivatives of temperature with respect to body position is necessary for evaluation of conduction. Attempts were made to obtain the derivatives by various analytical and graphical techniques. While these methods were in qualitative agreement, none was felt to give accurate results. Consequently, no conduction corrections were applied to the data.

It was felt to be desirable to obtain a qualitative understanding of the effects and to obtain some order of magnitude estimates of the errors introduced by conduction. The data from one pair of runs were analyzed at a number of times between 0.3 second and 3.45 seconds from nitrogen shutoff. Temperature distributions at several times are presented in figure 12. Since two runs were necessary for each test condition, the points presented do not necessarily form a continuous line at a given time. This fact is indicated by breaking the lines between sets of thermocouples. The temperature gradients were smallest at the earliest time and, in addition, the temperature distribution at the earliest time more closely approximated the equilibrium temperature distribution than at later times.

Representative curves of heating rate versus wall temperature are presented in figure 13. With the assumption that heat-transfer coefficient is not a function of wall temperature, these curves should be straight lines whose slope is equal (and opposite in sign) to the heat-transfer coefficient. The slope of the dashed line represents the heat transfer coefficient presented in the data. Estimated conduction corrections have been applied to some of the data and the corrected values are indicated by the filled symbols. The curve for thermocouple 2 is representative of the very low heating rate regions. Conduction heat transfer apparently increased faster than convective heat transfer decreased as the model heated with the result that the curve is far from the ideal straight line. It can be seen that the corrected values still do not define a straight line but do indicate that the correct heat-transfer coefficient is somewhere between the value presented and the theoretical value which would be represented by a line having a slope twice that of the dashed line.

The curve presented for thermocouple 5 is typical of the high heating rate corner regions. Conduction was not calculated in the corner because of the complicated shape and the fact (as mentioned above) that the temperature distribution curves were not continuous across the corner. If the temperature distributions had been the same at the time data were evaluated and at equilibrium, conduction at these times would also have been the same. Since heat-transfer coefficient is determined from the slope of the curve, heat-transfer coefficient would have been correct even though the values of heating rate were incorrect. Qualitatively, it can be seen in figure 12 that both the first and second derivatives of the temperature-distribution curve are negative at all times for the corners. Conduction corrections would therefore tend to raise heating rate for all values of wall temperature including equilibrium. Because of the similarity between the temperature distribution curves at equilibrium and at the earliest time, it is felt that the slope of the corrected curve would not be greatly different from the slope of the dashed line in figure 13. The data presented for the corner region are therefore felt to have only small errors.

Thermocouple 8 was at the nominal stagnation point. For all times except equilibrium the thermocouple adjacent to 8 in the $\varphi = 90^{\circ}$ plane measured a higher temperature than thermocouple 8. As a result, the conduction correction changed signs as the wall temperature increased. The corrected points show some scatter about a line with 30 percent less slope than the dashed line. Recovery temperature should be indicated by the wall temperature at which heating rate is zero and the corrected line indicates a recovery temperature much closer to the theoretical value than does the equilibrium temperature. It should be emphasized that the temperature differences on the front face were not much larger than the possible errors estimated for the measurements and that small errors in the temperatures could have caused large errors in the conduction estimates.

Over most of the model, the conduction patterns were qualitatively similar at equilibrium and at 0.3 second from nitrogen shutoff. It was therefore felt that the data reduction technique used gave a more accurate value for heat-transfer coefficient than would have been given if equilibrium wall temperature had been replaced with a calculated recovery temperature in the data reduction equation.

REFERENCES

1. Chapman, Dean R.: An Approximate Analytical Method for Studying Entry Into Planetary Atmospheres. NASA TN 4276, 1958.

2. Chapman, Dean R.: An Analysis of the Corridor and Guidance Requirements for Supercircular Entry Into Planetary Atmospheres. NASA TR R-55, 1959.

3. Davy, William C., and Seiff, Alvin: A Study of the Stability and Performance of Some Unsymmetrical Truncated Conical Configurations for Lifting Re-entry. NASA TM X-504, 1961.

4. Stine, Howard A., and Wanlass, Kent: Theoretical and Experimental Investigation of Aerodynamic Heating and Isothermal Heat-Transfer Parameters on a Hemisphere Nose With Laminar Boundary Layer at Supersonic Mach Numbers. NACA TN 3344, 1954.

5. Nestler, D. E., and Goetz, R.: Survey of Theoretical and Experimental Determination of Skin Friction in Compressible Boundary Layers; Part III - Effect of Axial Variation of Local Pressure and Surface Temperature for Laminar Boundary Layer. General Electric Document 59SD339, 1959.

6. Fay, J. A., and Riddell, F. R.: Theory of Stagnation Point Heat Transfer in Dissociated Air. Jour. Aero. Sci., vol. 25, no. 2, Feb. 1958, pp. 73-85.

7. Shenker, Henry, Lauritzen, John I., Jr., Corruccini, Robert J., and Lonberger, S. T.: Reference Tables for Thermocouples. National Bureau of Standards Circular 561, Apr. 27, 1955.

8. Loving, Donald L., and Katzoff, S.: The Flourescent-Oil Film Method and Other Techniques for Boundary-Layer Flow Visualization. NASA MEMO 3-17-59L, 1959.

9. Sykes, C., and Wilkinson, H.: The Specific Heat of Nickel From 100° to 600° C. Proceedings of the Physical Socity, vol. 50, 1938, pp. 834-851.

10. Wise, E. M., and Schaefer, R. H.: The Properties of Pure Nickel. I. Metals and Alloys. Sept. 1942, pp. 424-428.

11. Owen, P. R., and Randall, D. G.: Boundary Layer Transition on a Sweptback Wing. RAE Tech Memo. Aero 277, May 1952.

12. Boltz, Frederick W., Kenyon, George C., and Allen, Clyde Q.: Effects of Sweep Angle on the Boundary-Layer Stability Characteristics of an Untapered Wing at Low Speeds. NASA TN D-338, 1960.

13. van Driest, E. R. and McCauley, W. D.: The Effect of Controlled Three-Dimensional Roughness on Boundary Layer Transition at Supersonic Speeds. North American Aviation, Inc., Missile Division MD59-115, 1958.

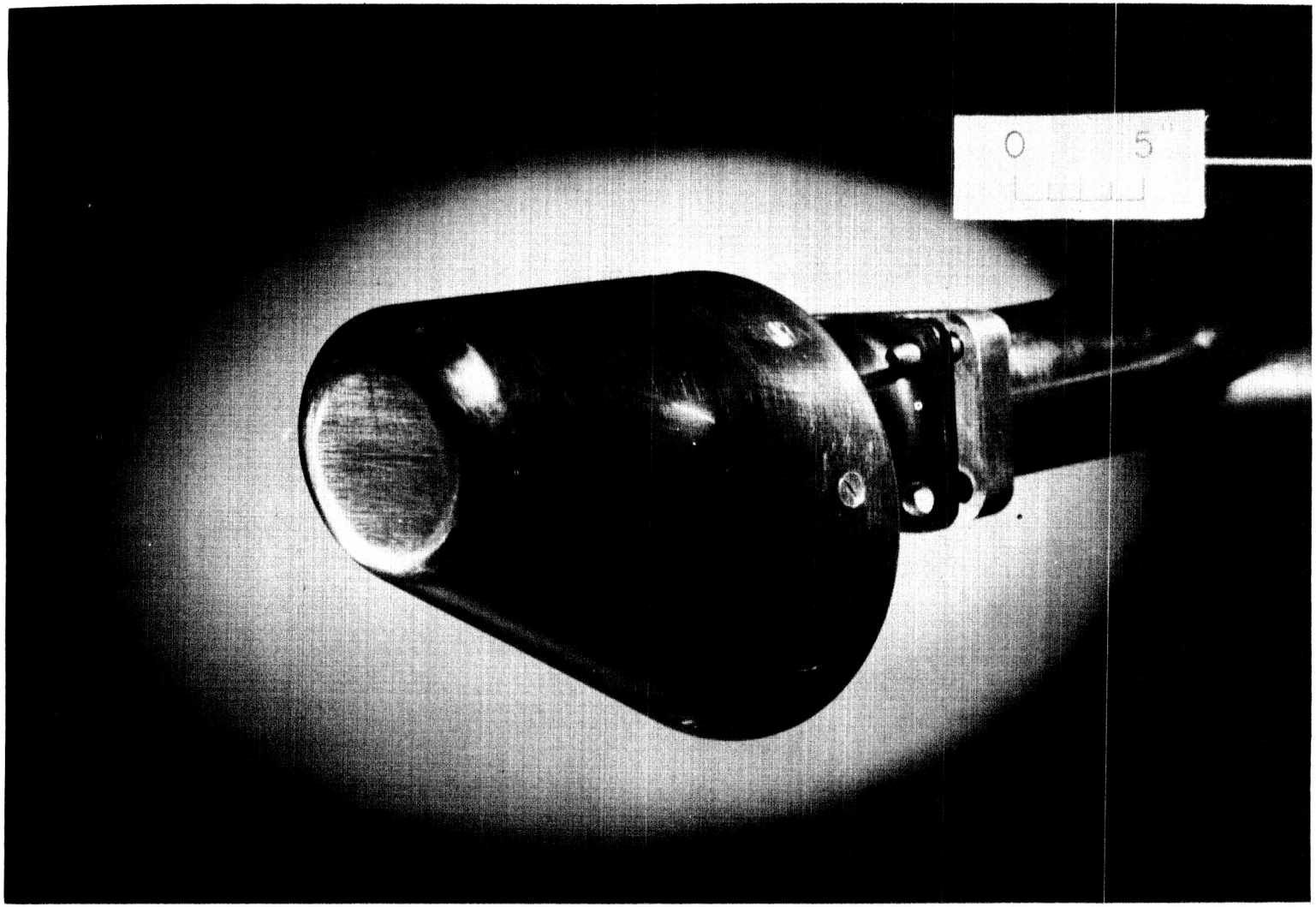

A-26643

Figure 1.- Photograph of heat-transfer model.

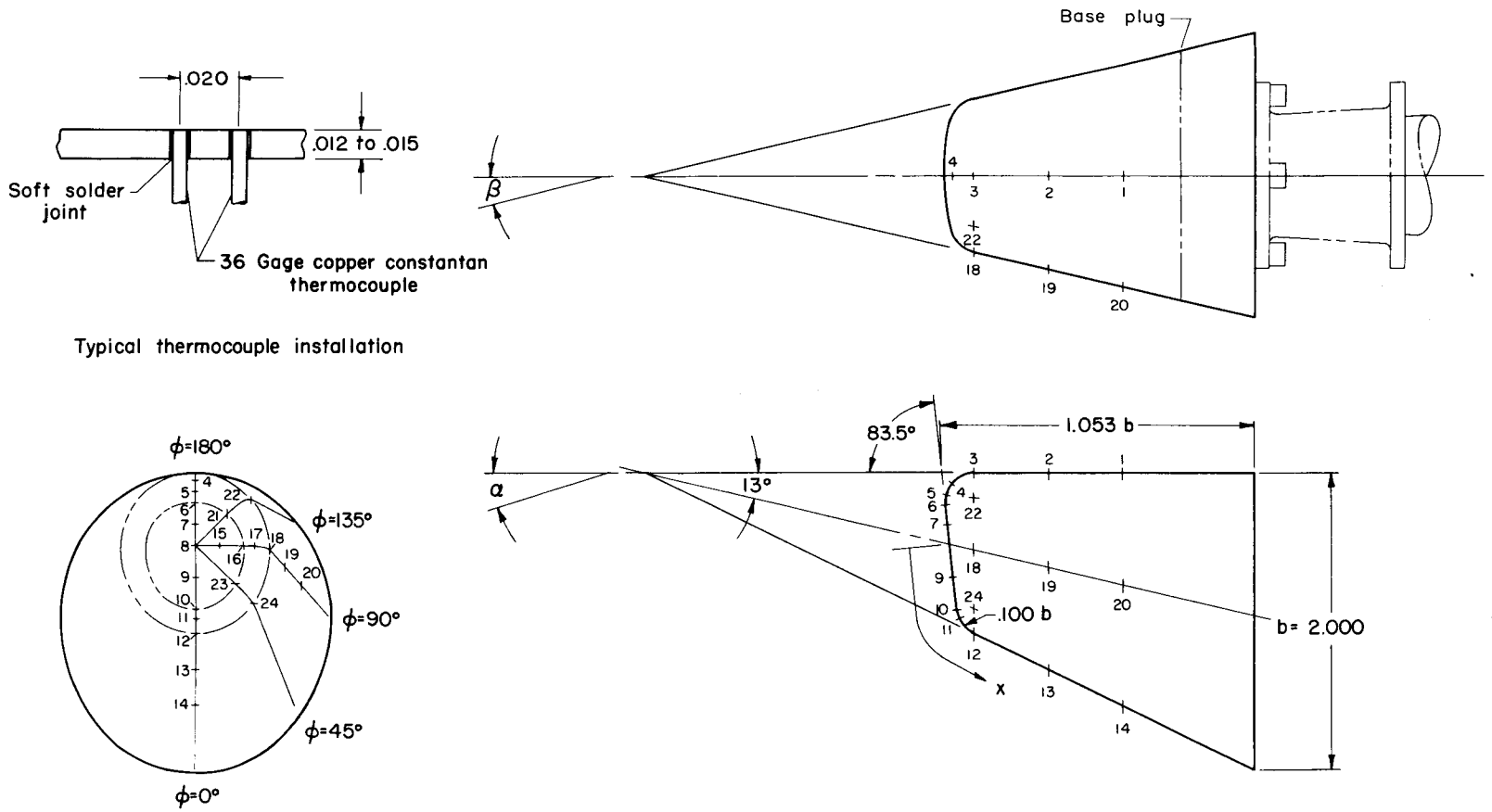

Figure 2.- Geometry and instrumentation of model.

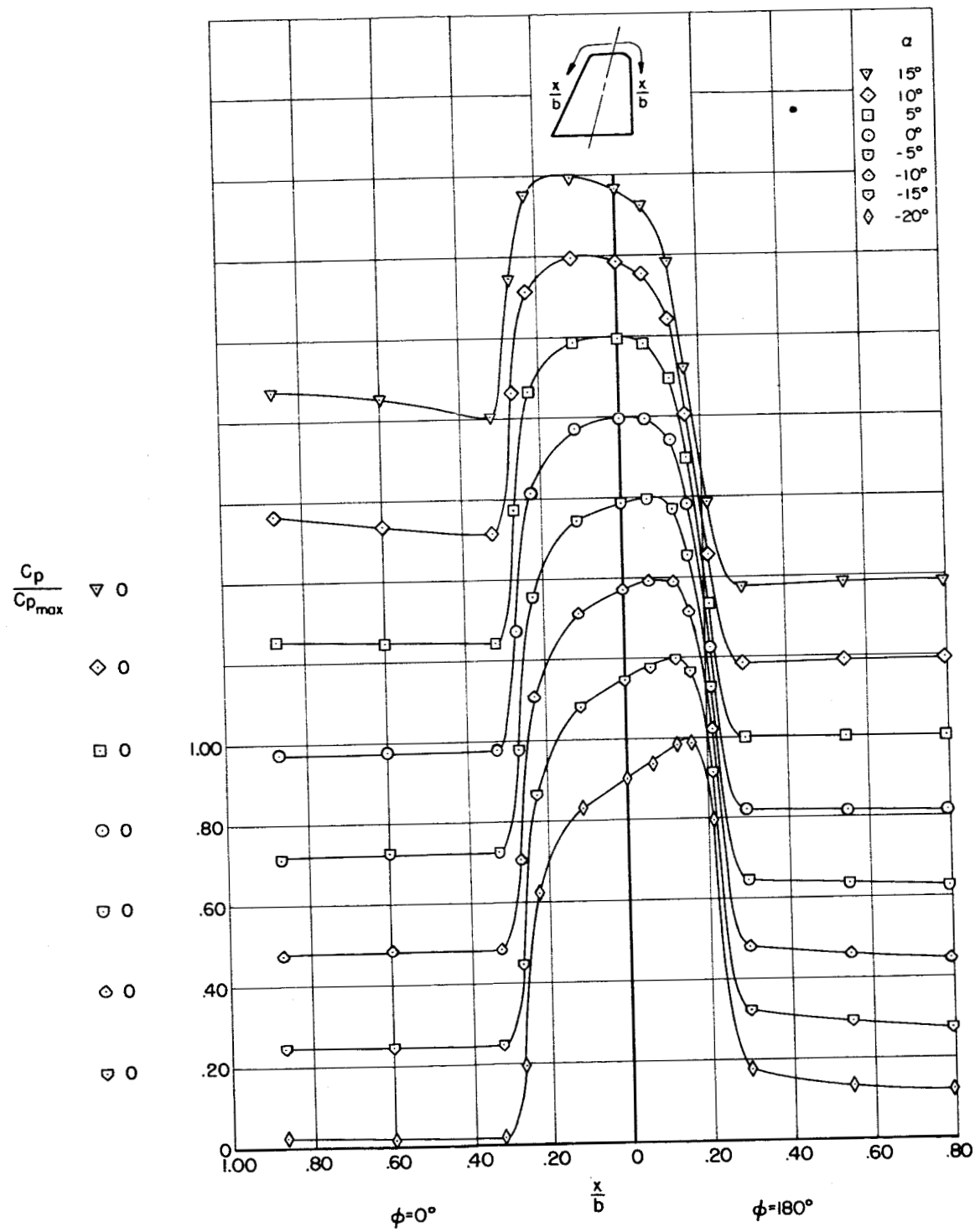

(a) Variation with angle of attack in plane of symmetry.

Figure 3.- Pressure distribution at $M = 4.0$ and $Re_{b_\infty} = 0.88(10)^6$.

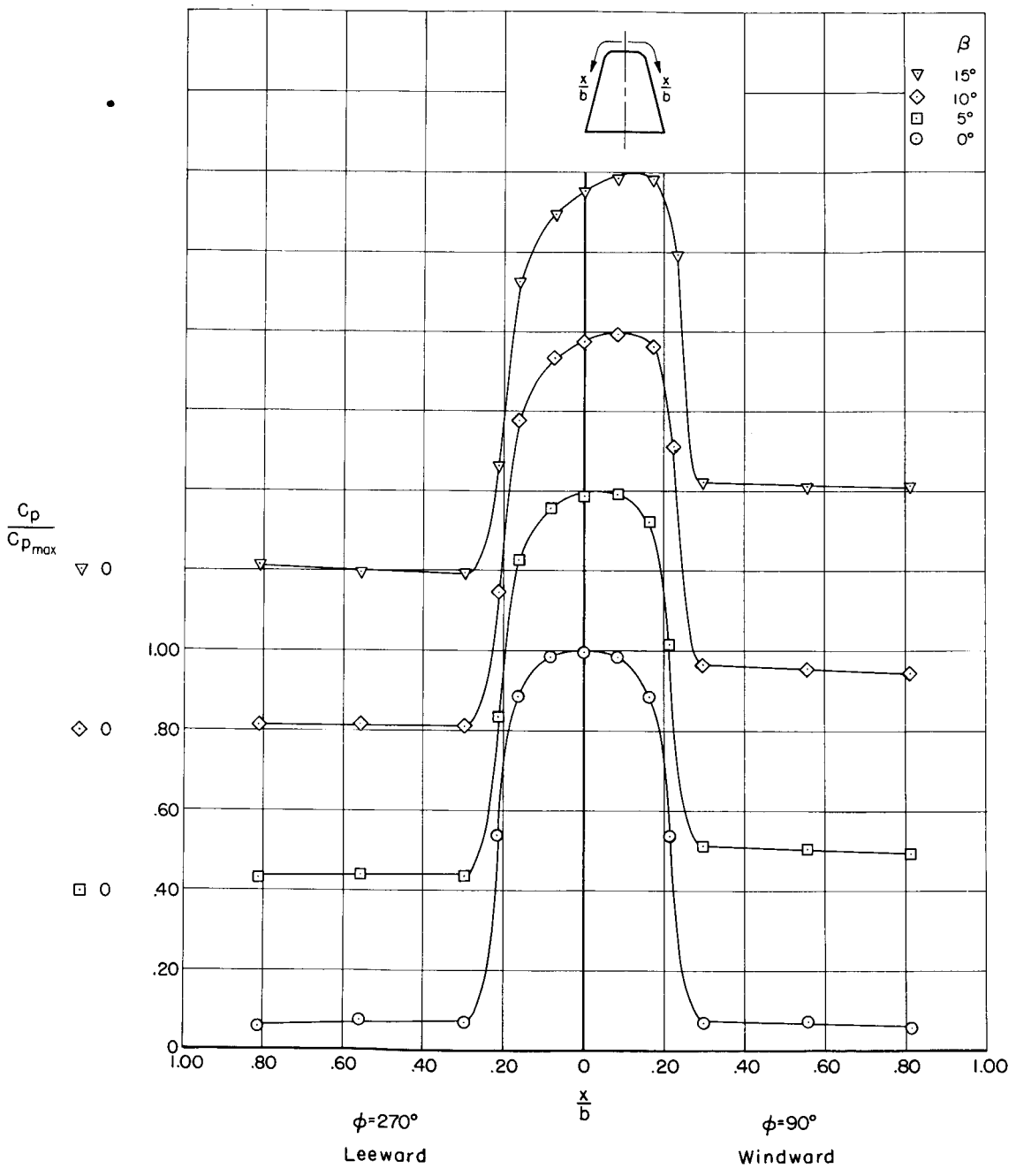

(b) Variation with angle of sideslip in $\varphi = 90^{\circ}$ plane.

Figure 3.- Concluded.

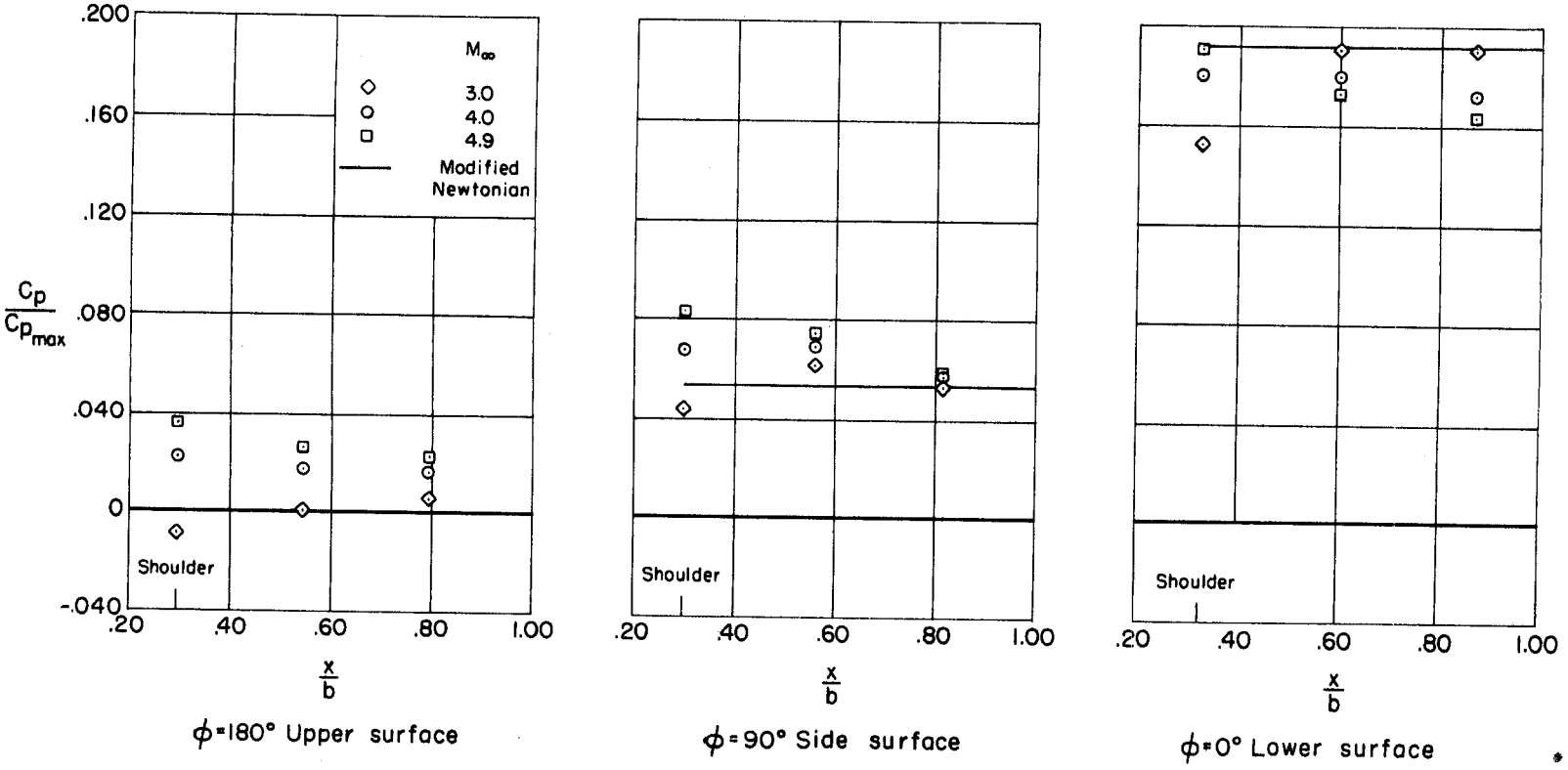

Figure 4.- Variation of afterbody pressures with Mach number at $\alpha = 0$ and $\beta = 0$.

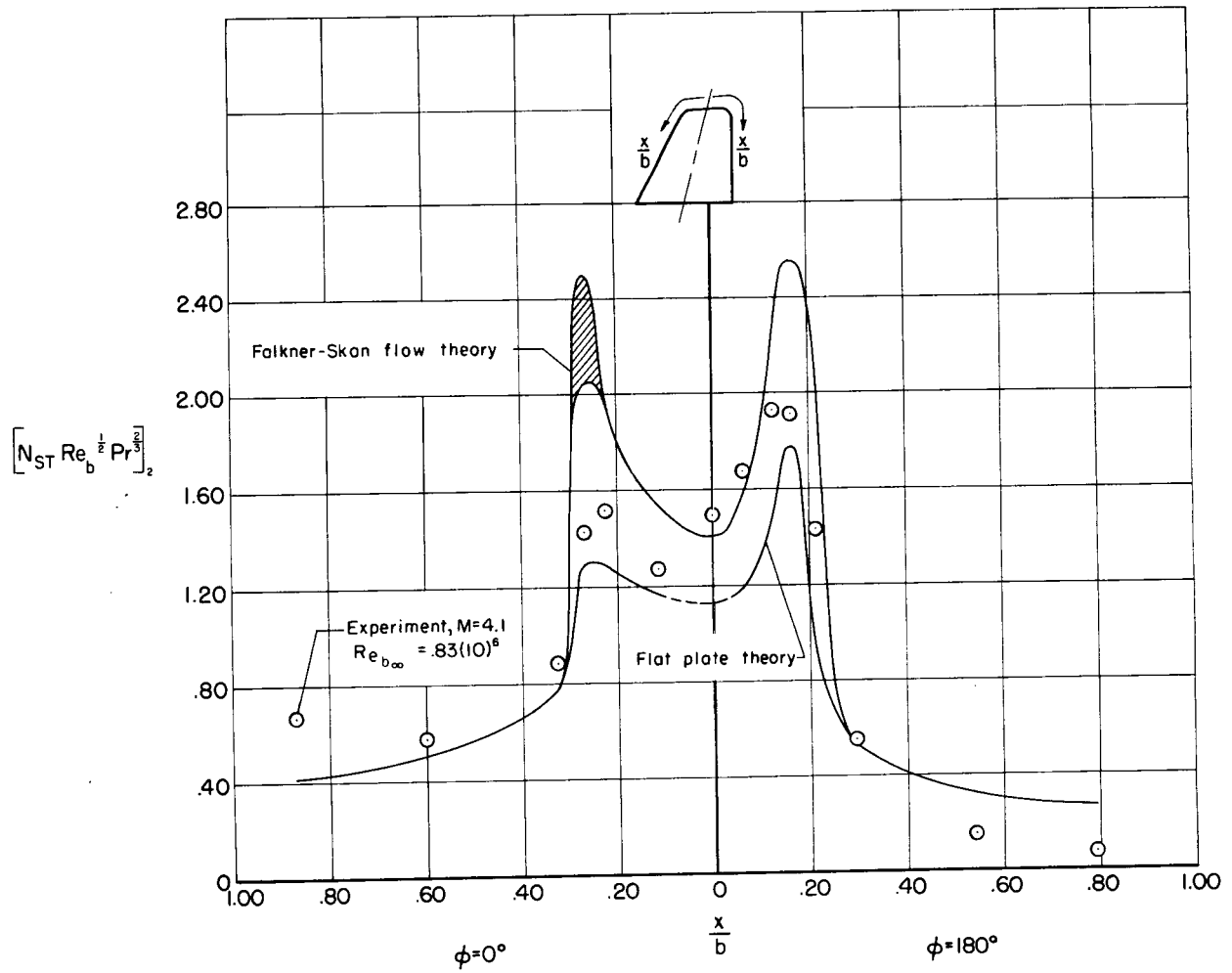

(a) Plane of symmetry.

Figure 5.- Comparison between heat-transfer distribution and theory at $M = 4.1$ and $Re_{b_\infty} = 0.83(10)^6$ at $\alpha = 0$ and $\beta = 0$.

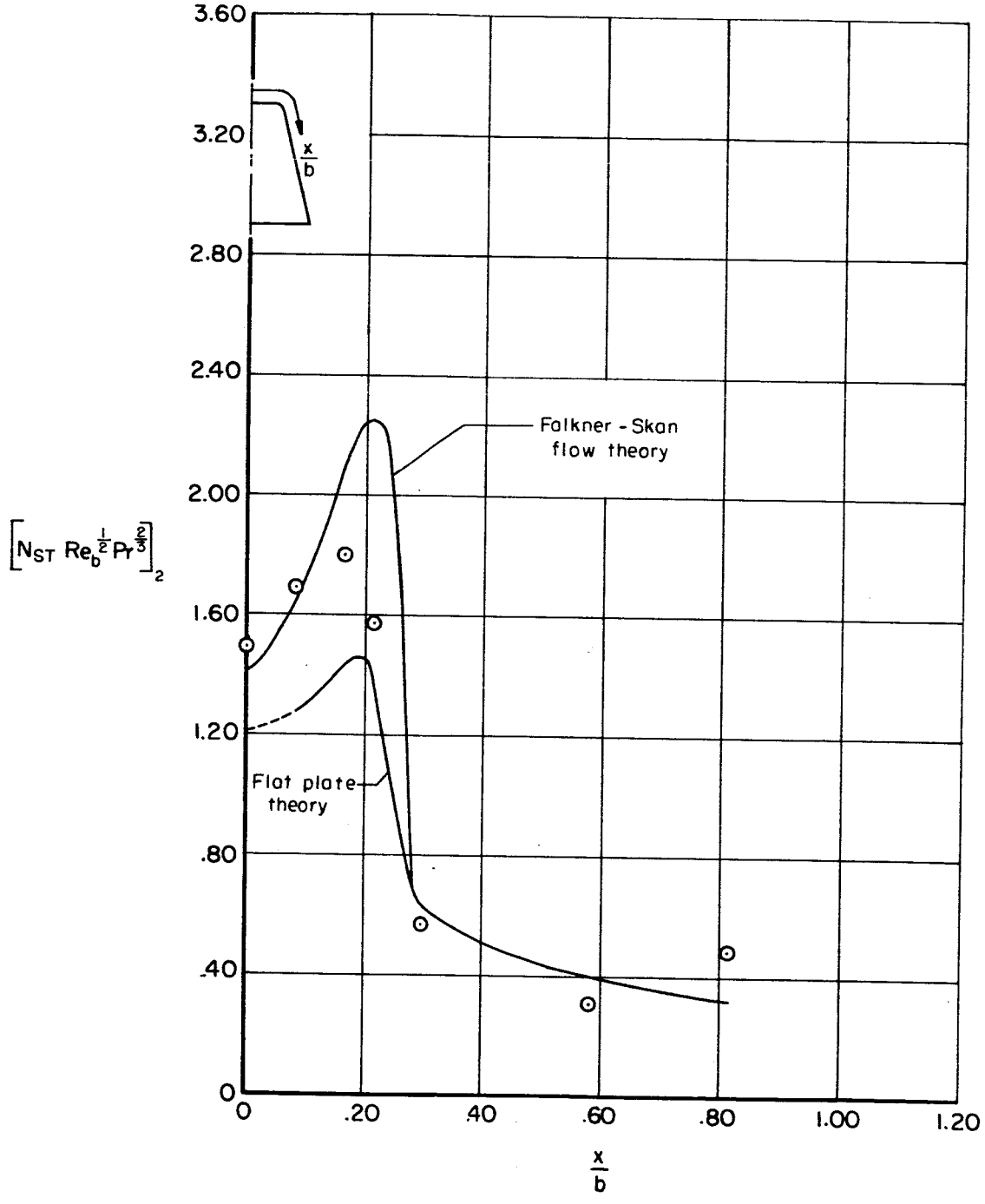

(b) $\varphi = 90^\circ$ plane.

Figure 5.- Concluded.

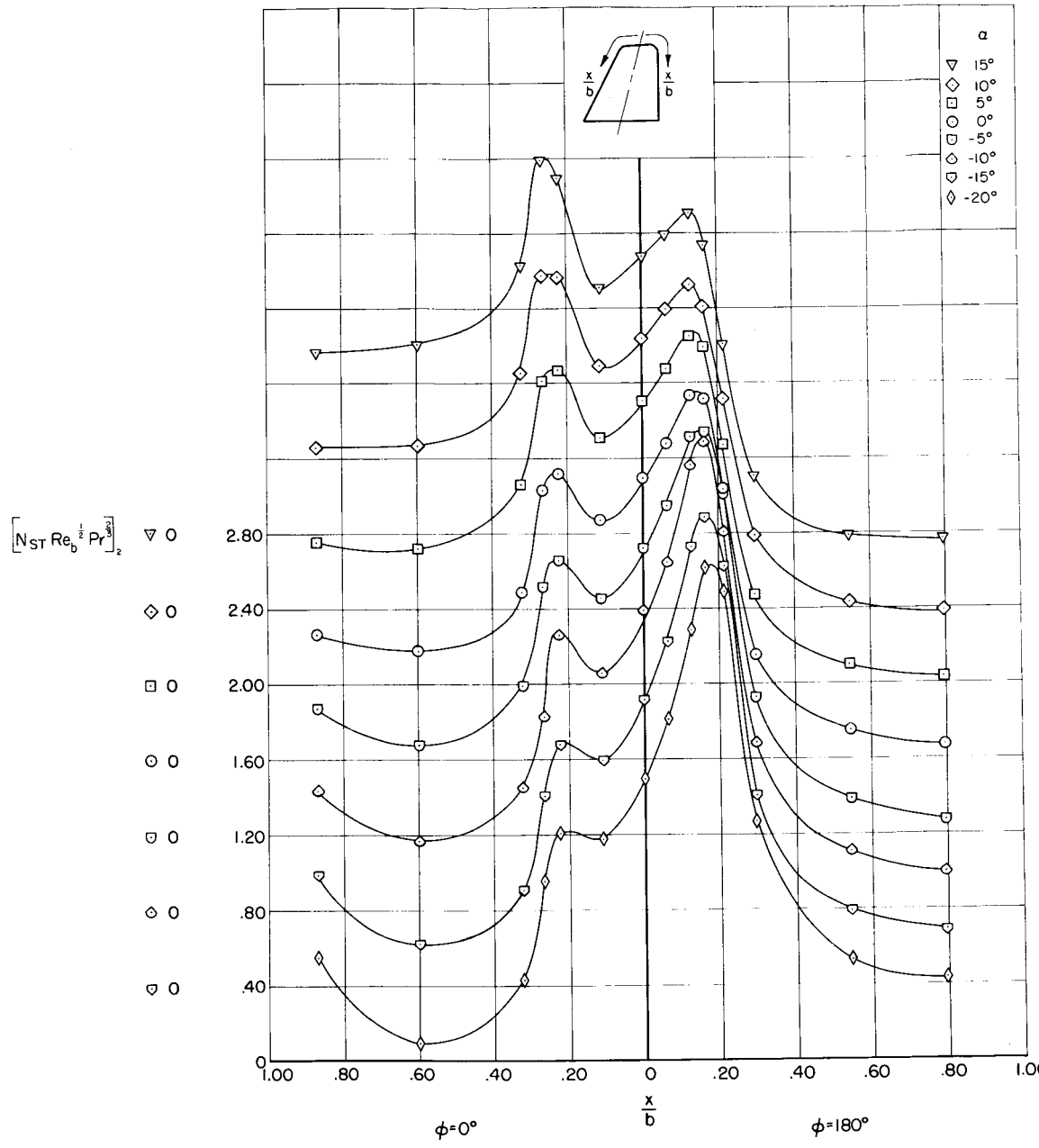

(a) Variation with angle of attack in plane of symmetry ($\beta = 0$).

Figure 6.- Heat-transfer distribution at $M = 4.1$ and $Re_{b_\infty} = 0.83(10)^6$.

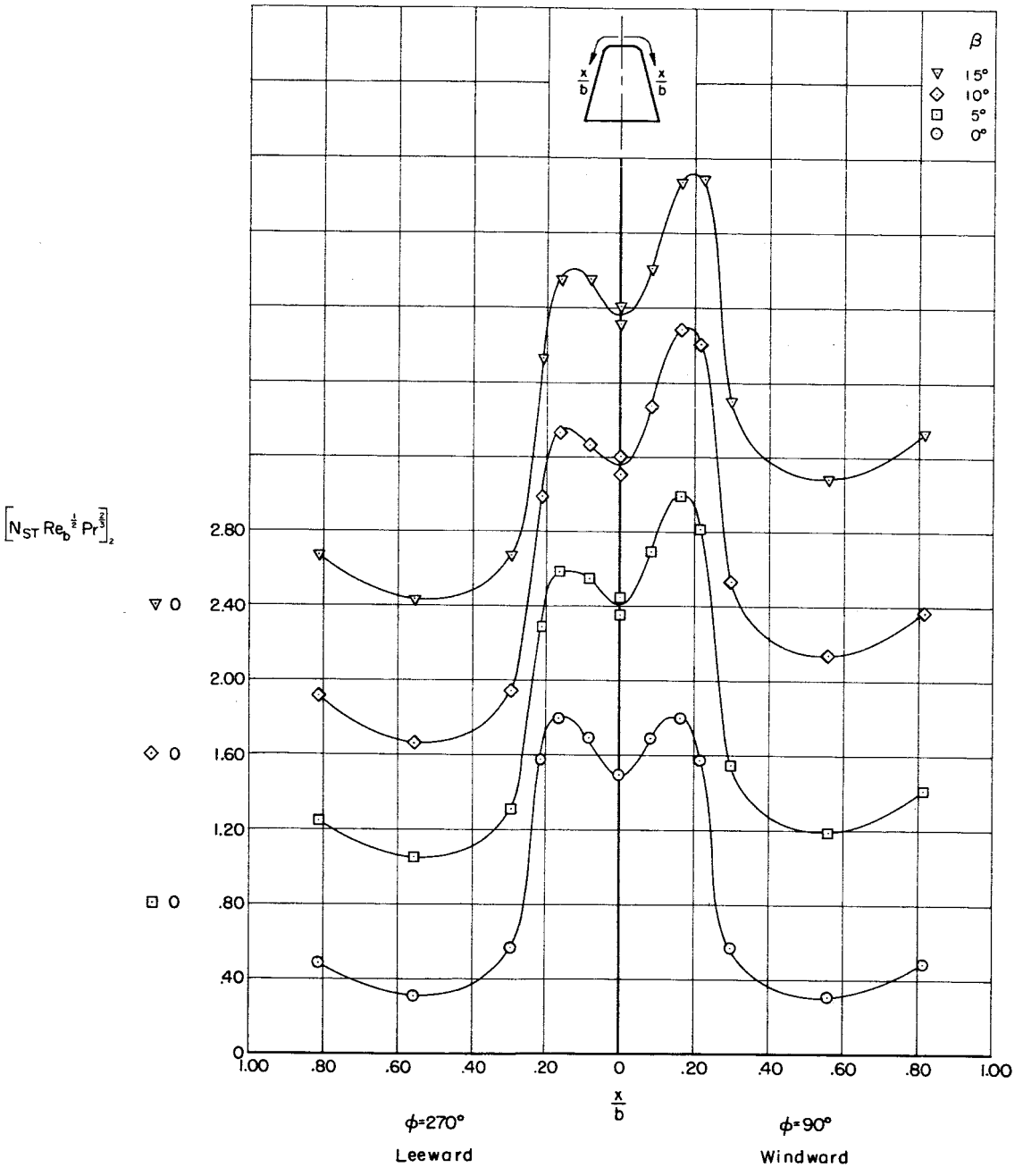

(b) Variation with angle of sideslip in $\varphi = 90^{\circ}$ plane ($\alpha = 0$).

Figure 6.- Concluded.

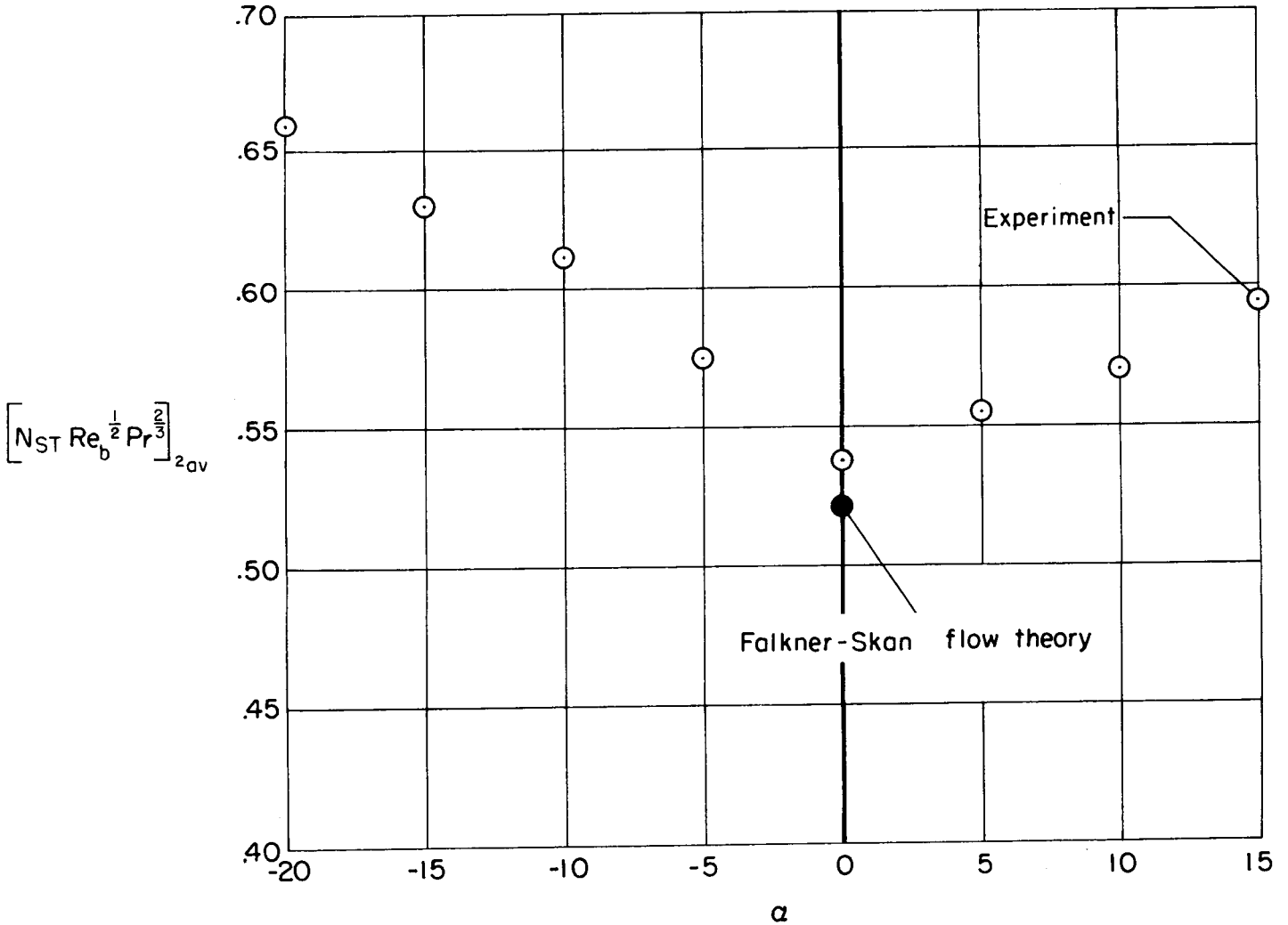

Figure 7.- Variation of average heat-transfer parameter with angle of attack at $M = 4.1$, $Re_{b_\infty} = 0.83(10)^6$, and $\beta = 0$.

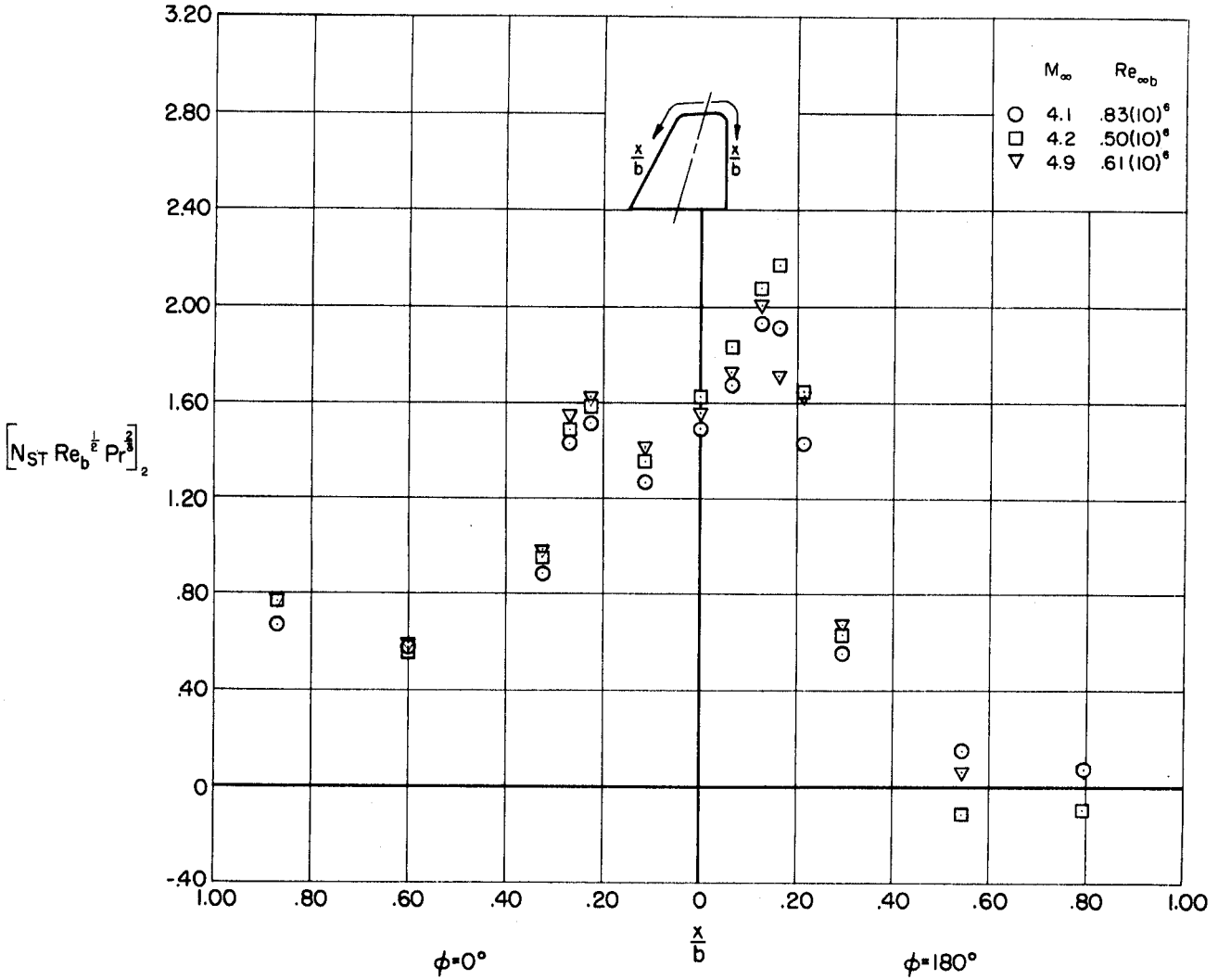

Figure 8.- Variation of heat-transfer parameter with Mach and Reynolds numbers at $\alpha = 0$ and $\beta = 0$.

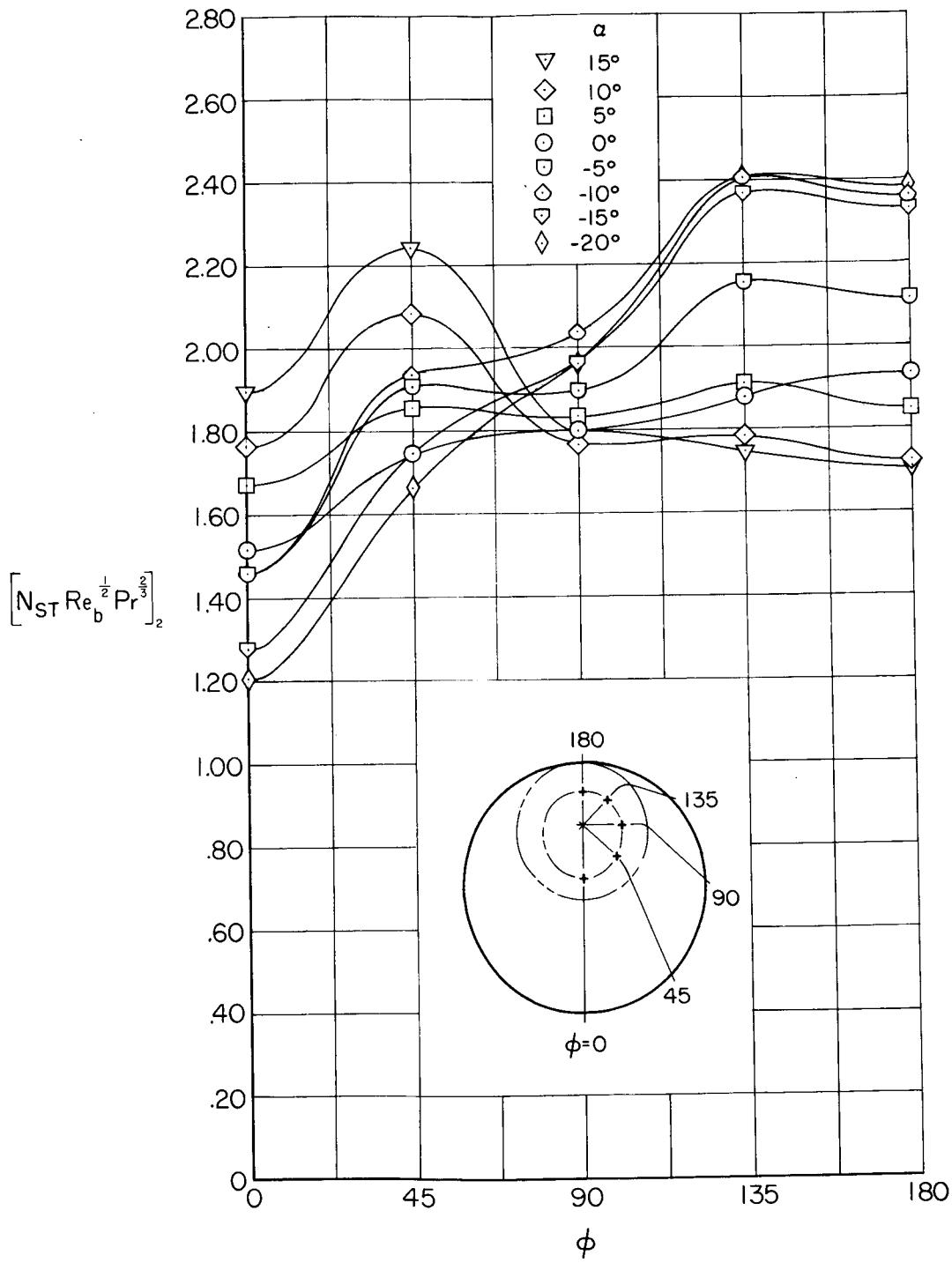

(a) Beginning of corner.

Figure 9.- Peripheral variation of heat-transfer parameter with angle of attack at $M = 4.1$, $Re_{b_\infty} = 0.83(10)^6$, and $\beta = 0$.

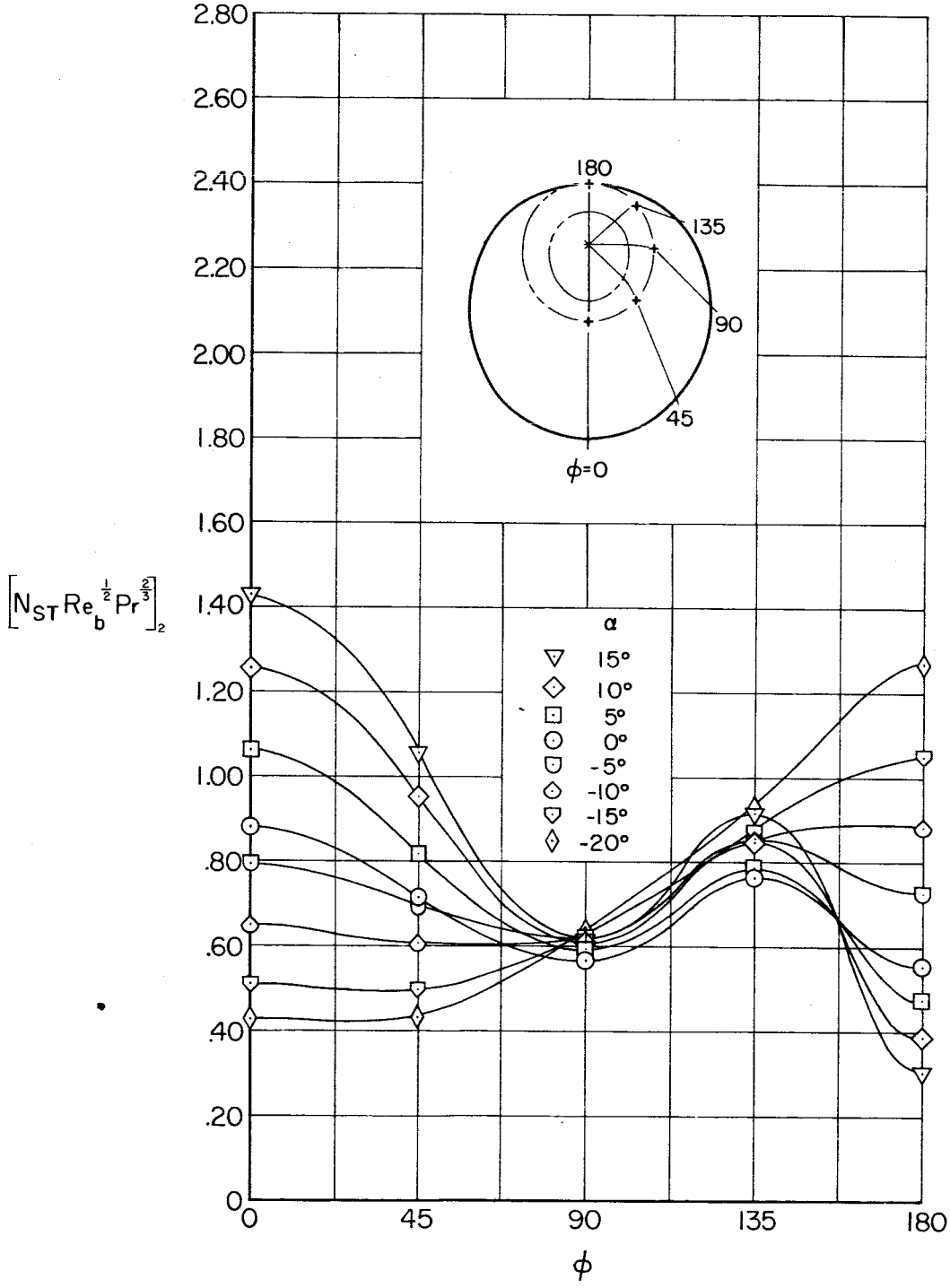

(b) End of corner.

Figure 9.- Concluded.

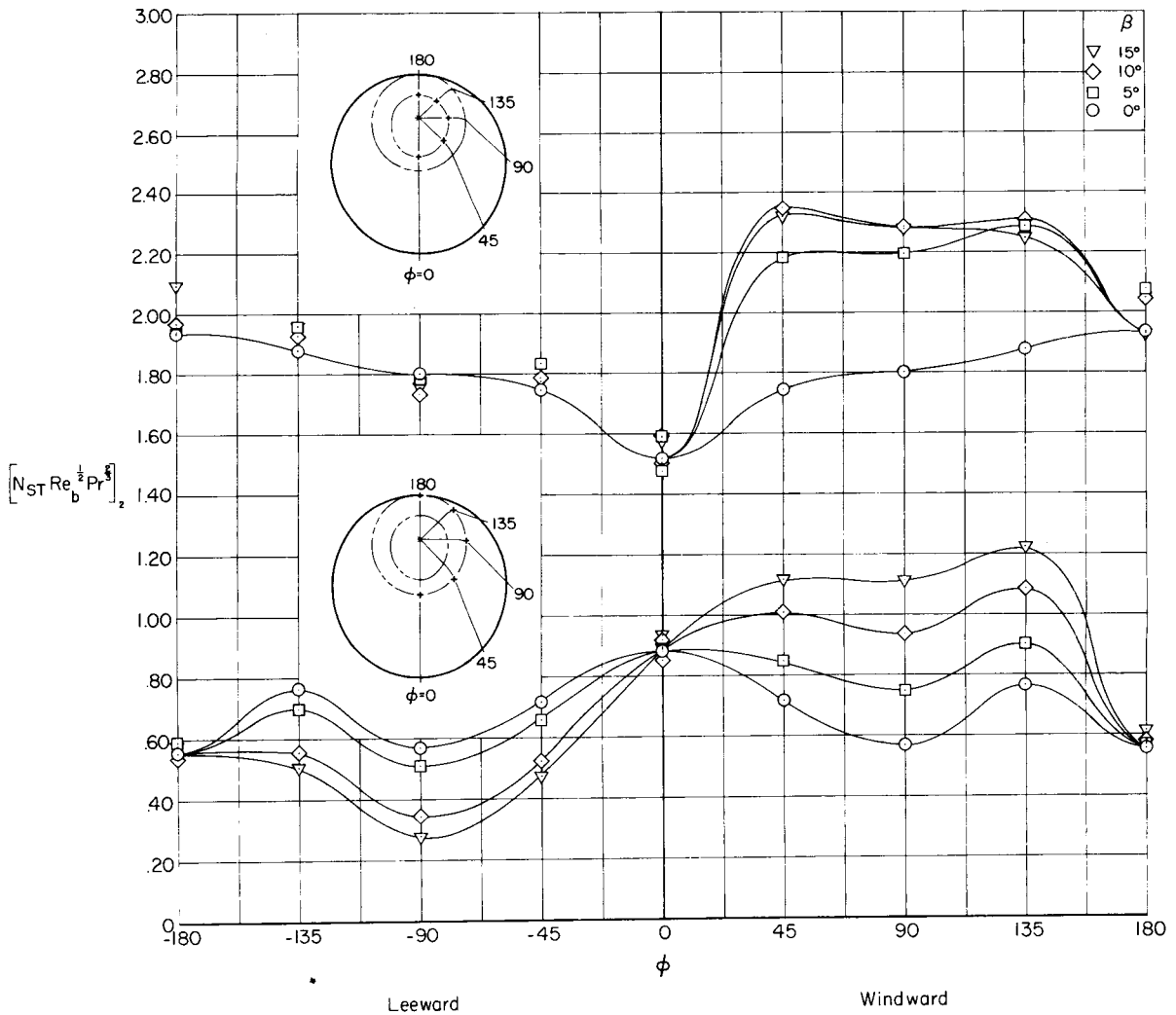

Figure 10.- Peripheral variation of heat-transfer parameter at beginning and end of corner with angle of sideslip at $M = 4.2$, $Re_{b_\infty} = 0.77(10)^6$, and $\alpha = 0$.

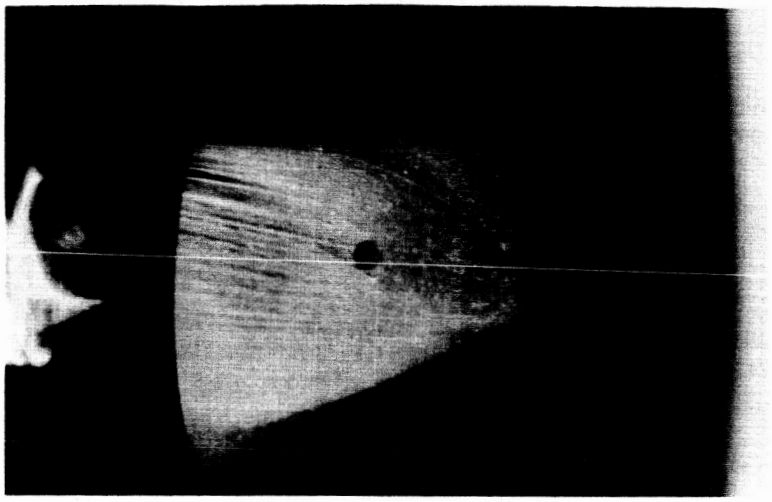

(a) $\alpha = 0$, side.

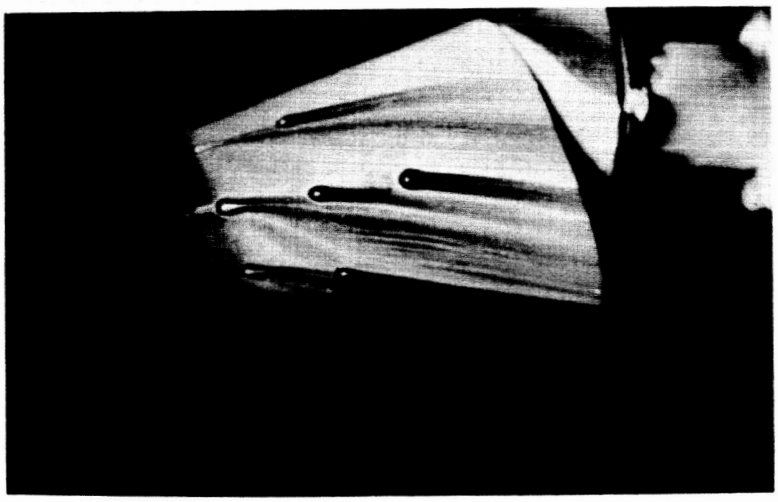

(b) $\alpha = -20^{\circ}$, side.

Figure 11.- Boundary-layer-flow visualization pictures at $M = 3.0$ and $Re_{b_\infty} = 1.3(10)^6$.

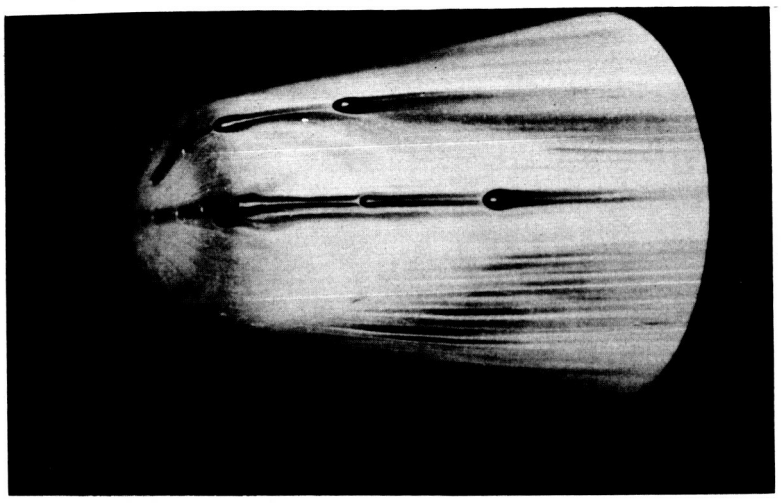

(c) $\alpha = -20^{\circ}$, bottom.

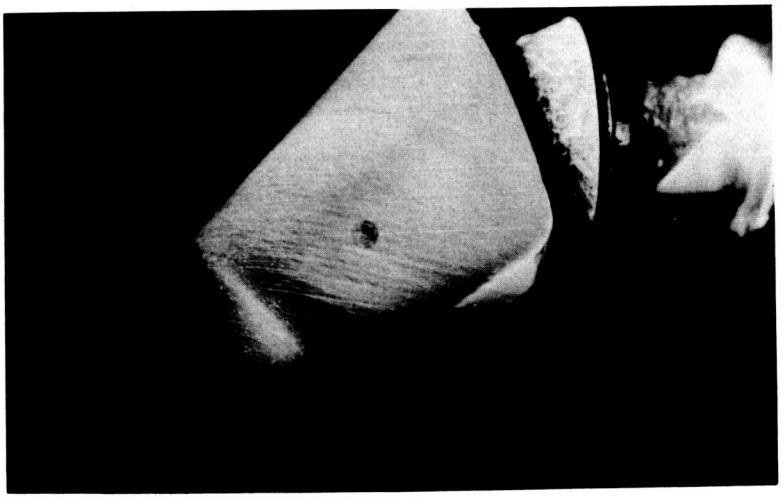

(d) $\alpha = 20^{\circ}$, side.

Figure 11.- Continued.

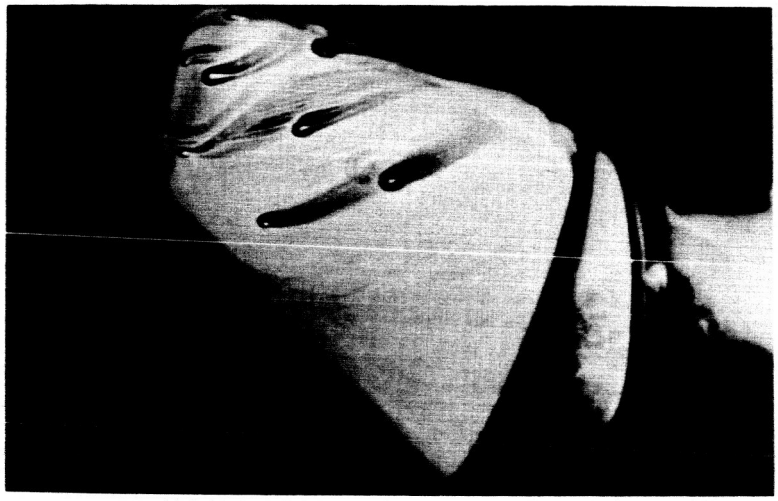

(e) $\alpha = 20^{\circ}$, side.

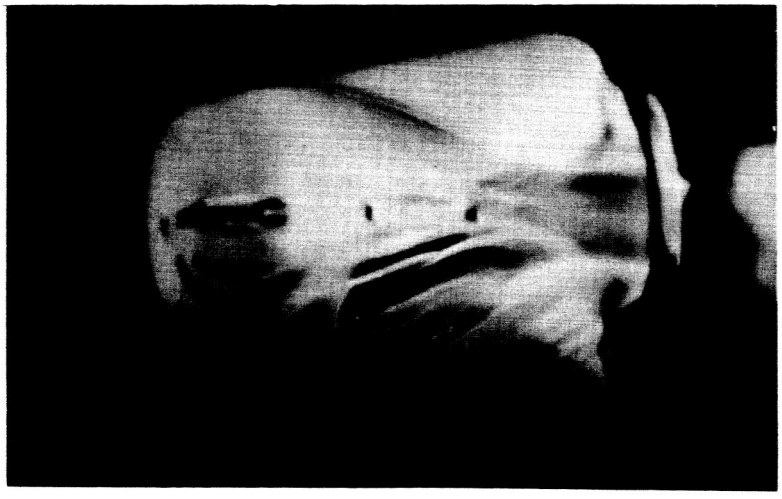

(f) $\alpha = 20^{\circ}$, top.

Figure 11.- Concluded.

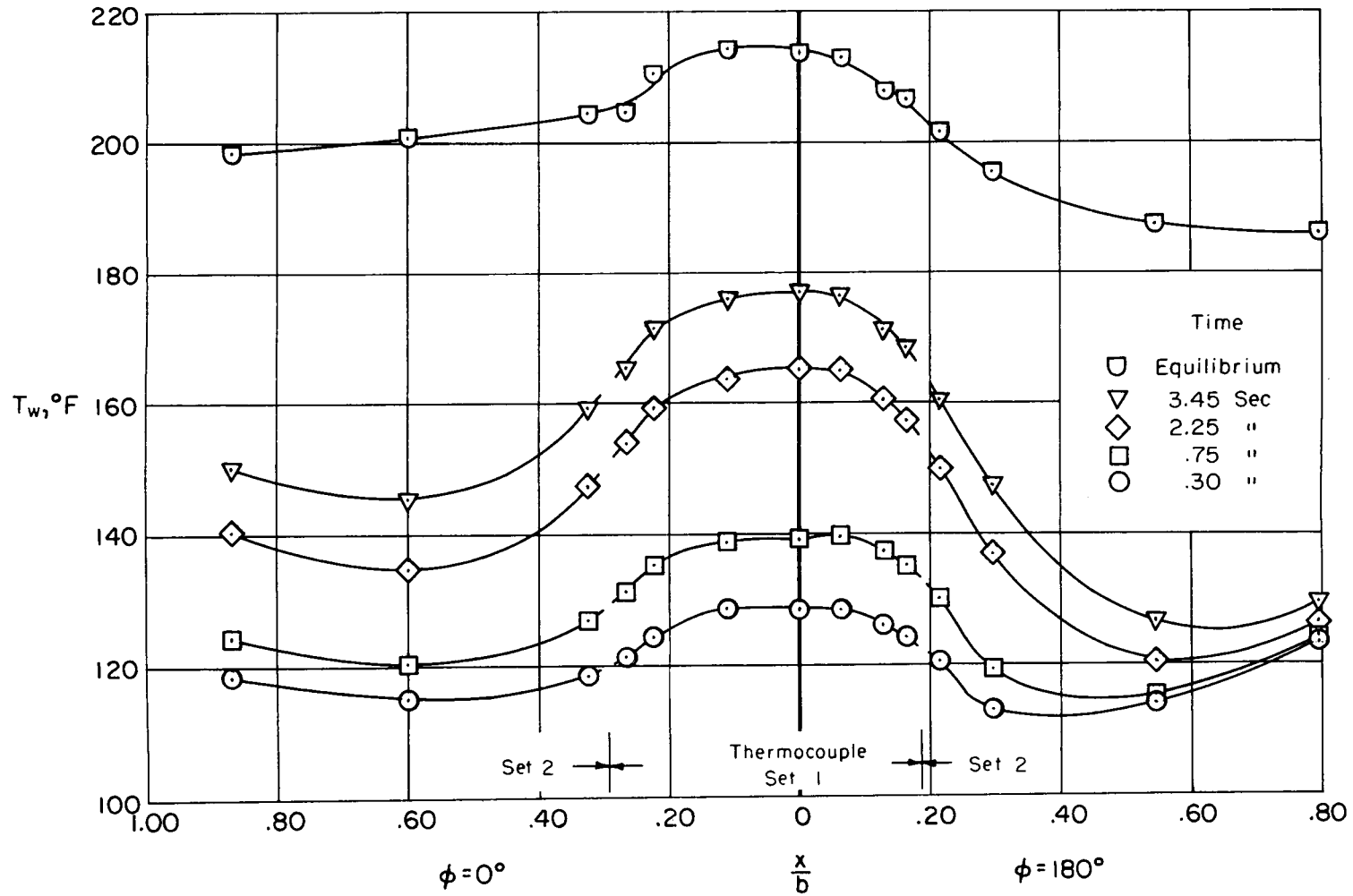

(a) Plane of symmetry.

Figure 12.- Temperature distribution as a function of time at $M = 4.1$, $Re_{b_\infty} = 0.83(10)^6$, $\alpha = 0$, and $\beta = 0$.

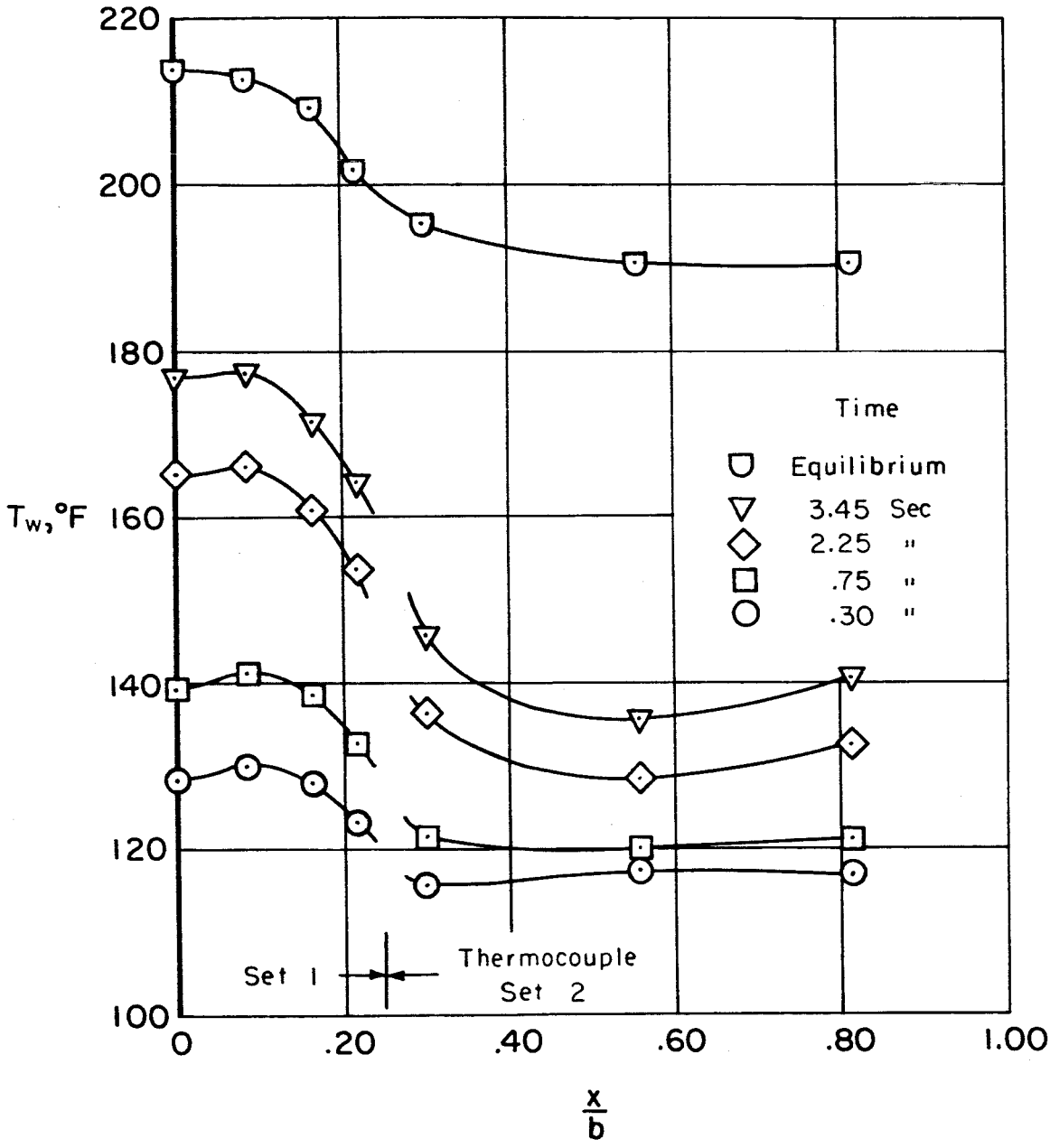

(b) $\varphi = 90^{\circ}$ plane.

Figure 12.- Concluded.

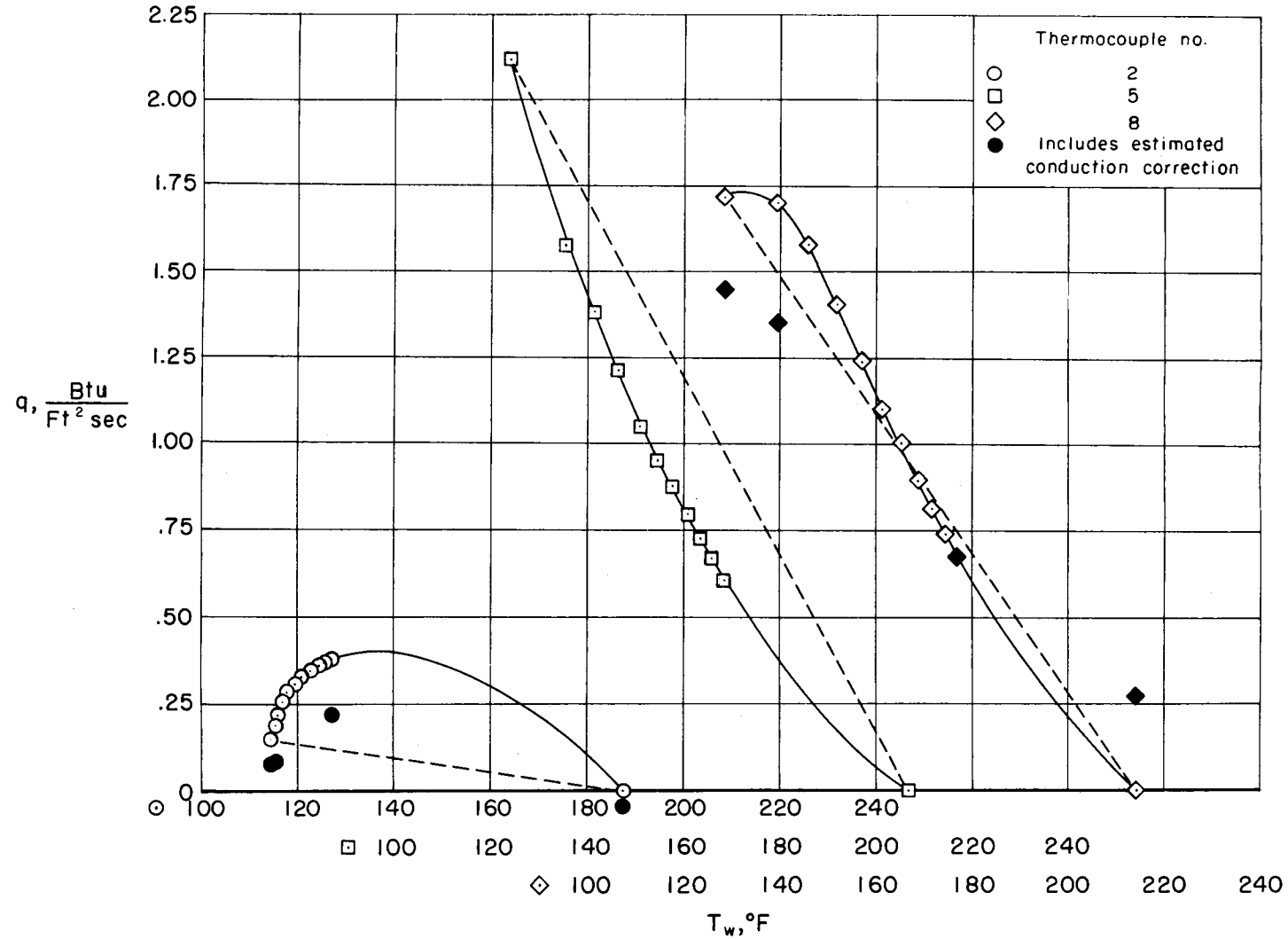

Figure 13.- Variation of heating rate with wall temperature for representative thermocouples at $M = 4.1$, $Re_{b_\infty} = 0.83(10)^6$, $\alpha = 0$, and $\beta = 0$.